Contrib Mineral Petrol (1997) 129: 308–325

John D. Clemens · Giles T.R. Droop · Gary Stevens

High-grade metamorphism, dehydration and crustal melting: a reinvestigation based on new experiments in the silica-saturated portion of the system $KAlO_2$–MgO–SiO_2–H_2O–CO_2 at $P \leq 1.5$ GPa

Received: 28 November 1996 / Accepted: 25 June 1997

Abstract The system $KAlO_2-MgO-SiO_2-H_2O-CO_2$ has long been used as a model for the processes of granulite-facies metamorphism and the development of orthopyroxene-bearing mineral assemblages through the breakdown of biotite-bearing assemblages. There has been considerable controversy regarding the role of carbon dioxide in metamorphism and partial melting. We performed new experiments in this system (at pressures of 342 to 1500 MPa with T between 710 and 1045 °C and $X^{Fl}_{H_2O}$ between 0.05 and 1.00), accurately locating most of the dehydration and melting equilibria in P-T-$X^{Fl}_{H_2O}$ space. The most important primary result is that the univariant reaction Phl + Qtz + Fl = En + Sa + melt must be almost coincident with the fluid-absent reaction (Phl + Qtz = En + Sa + melt) in the CO_2-free subsystem. In conjunction with the results of previous measurements of CO_2 solubility in silicate melts and phase equilibrium experiments, our theoretical analysis and experiments suggest that CO_2 cannot act as a flux for partial melting. Crustal melting in the presence of H_2O–CO_2 mixed fluids will always occur at temperatures higher than with pure H_2O fluid present. Magmas produced by such melting will be granitic (s.l.) in composition, with relatively high SiO_2 and low MgO contents, irrespective of the H_2O–CO_2 ratio in any coexisting fluid phase. We find no evidence that lamprophyric magmas could be generated by partial fusion of quartz-saturated crustal rocks. The granitic melts formed will not contain appreciable dissolved CO_2. The channelled passage of hot CO_2-rich fluids can cause local dehydration of the rocks through which they pass. In rock-dominated (as opposed to fluid-dominated) systems, minor partial melting can also occur in veins initially filled with CO_2-rich fluid, as dehydration and local disequilibrium drive the fluid towards H_2O-rich compositions. However, CO_2 is unlikely to be a significant agent in promoting regional granulite-grade metamorphism, melting, magma generation, metasomatism or long-range silicate mass transfer in Earth's crust. The most viable model for the development of granulite-facies rocks involves the processes of fluid-absent partial melting and withdrawal of the melt phase to higher crustal levels.

J.D. Clemens (✉)
School of Geological Sciences, Kingston University,
Penrhyn Rd, Kingston-upon-Thames, Surrey, KT1 2EE, UK

G.T.R. Droop
Department of Earth Sciences, University of Manchester,
Oxford Rd, Manchester M13 9PL, UK

G. Stevens
Economic Geology Research Unit, University of Witwatersrand,
Johannesburg, Private Bag 3, WITS 2050, South Africa

Editorial responsibility: I. Parsons

Introduction

Interest in the system $KAlO_2-MgO-SiO_2-H_2O-CO_2$ stems from the fact that it represents the simplest model for the stability of biotite in subaluminous and metaluminous, quartz-saturated crustal rocks, under conditions appropriate to high-grade metamorphism or for the crystallization of intermediate to felsic magmas. This system has long been used as a model for understanding the processes of granulite-facies metamorphism and the development of orthopyroxene-bearing mineral assemblages through the breakdown of biotite-bearing assemblages (see, e.g. Bohlen et al. 1983; Grant 1986; Newton 1990). Recent calorimetric investigations (Robie and Hemingway 1984; Clemens et al. 1987; Circone and Navrotsky 1992) have yielded thermodynamic data for phlogopite that are consistent with the best available experimental results for the subsolidus equilibrium:

$$Phl + 3Qtz = 3En + Sa + H_2O \qquad [M]$$

(Clemens 1995). Note that all phase abbreviations used in this paper are from Kretz (1983); additional symbols used are Fl = supercritical fluid phase, M = silicate melt and Gl = glass (quenched melt). Recent experi-

mental studies (Vielzeuf and Clemens 1992; Clemens 1995) have clarified the stoichiometry and P–T locations of all silica-saturated equilibria in the CO_2-free subsystem ($KAlO_2-MgO-SiO_2-H_2O$).

There has been considerable controversy regarding the role of carbon dioxide in metamorphism and partial melting of Earth's crust. The presence of CO_2-rich fluid inclusions in some granulite-facies minerals led to the hypothesis of "CO_2 flushing" (Touret 1970; Newton et al. 1980), in which granulite-facies mineral assemblages would be produced through relatively low-temperature, subsolidus, dehydration reactions. The controversy has been fuelled more recently by reports of experimental evidence for CO_2-enhanced partial melting of the assemblage phlogopite + quartz in the model system $KAlO_2-MgO-SiO_2-H_2O-CO_2$ (Peterson and Newton 1989b, 1990). The analogous processes in the crust would lead to the formation of granulite-facies rocks at temperatures usually considered characteristic of the amphibolite facies. Granulites would thus be indicative not of unusually high temperatures, but of the influx of carbonic fluids. Moreover, the similarity of their low-temperature melts to the compositions of some calc-alkaline lamprophyres led Peterson and Newton (1989b, 1990) to suggest that such magmas might be generated by the introduction of CO_2-rich fluids, providing a mechanism for large-scale mass transfer in the deep crust. These ideas have been highly influential, but there are aspects of Peterson and Newton's results that are hard to reconcile with other available data.

In the present paper, we present new experimental data (on the T–$X^{Fl}_{H_2O}$ phase relations among reactions involving phlogopite in the system with H_2O–CO_2 fluids present) that cast considerable doubt on the findings and interpretations of Peterson and Newton (1989b, 1990). Below, we will discuss the importance of this system for understanding high-grade metamorphism, introduce theoretical aspects of the phase relations, evaluate previous work and report our own experimental results. Finally, we discuss some of the important implications for the petrogenesis of granulites and charnockites and for the production of granitoid magmas by crustal melting.

Carbonic metamorphism and the granulite facies

The presence or absence, nature and compositions of fluids in the granulite facies are crucial issues in the evolution of rocks at these highest grades of crustal metamorphism. Granulite-facies mineral assemblages indicate low values of a_{H_2O} at the peak of metamorphism. These assemblages commonly occur in rocks whose protoliths were hydrous, and explanations for this have produced two main categories of model – fluid-absent and fluid-present schemes. Below, we summarize their important features and evaluate these models.

The common occurrence of nearly pure, high-density CO_2 in metamorphic fluid inclusions in granulites (Rudnick et al. 1984; Touret 1985), compared with mixed to H_2O-rich fluid inclusions from amphibolite-facies rocks, resulted in the hypothesis that granulite assemblages are produced through dehydration by the flux of hot CO_2-rich fluids through the crust (Touret 1971; Collerson and Fryer 1978; Newton et al. 1980). At low values of a_{H_2O}, dehydration reactions are displaced toward lower T. Thus, CO_2 influx could produce the transition from amphibolite to granulite facies without a temperature increase.

This mechanism has been proposed for the development of granulites and charnockites (see, e.g. Newton et al. 1980). In this model, migmatic textures in granulites are attributed to partial melting induced by an H_2O-rich fluid front that moves ahead of the carbonic fluid front.

Fluid-absent granulite formation occurs at much higher T. The absence of a pervasive fluid phase during the peak of metamorphism is supported by grade-independent variations in a_{H_2O} in the granulites (Edwards and Essene 1988), the H_2O and CO_2 contents of granulite-grade cordierites (Carrington and Harley 1996) and layer-scale heterogeneities in C isotopic composition in graphitic granulites (Venneman and Smith 1992). Here, the low a_{H_2O} is achieved through anatectic processes (e.g. Phillips 1980; Powell and Downes 1990; Stevens and Van Reenen 1992; Sighinolfi and Gorgoni 1978).

Fluid-absent partial melting reactions consume hydrous silicates and produce H_2O-undersaturated granitoid magmas (Fyfe 1973; Clemens 1990). Many experimental studies have confirmed the viability of this mechanism of granulite formation (Rutter and Wyllie 1988; Beard and Lofgren 1991; Rapp et al. 1991; Rushmer 1991; Sen and Dunn 1994; Skjerlie and Johnston 1993; Rapp and Watson 1995; Vielzeuf and Montel 1994; Patiño Douce and Beard 1995, 1996; Stevens et al. 1995; LeBreton and Thompson 1988; Vielzeuf and Holloway 1988; Patiño Douce and Johnston 1991; Carrington and Harley 1995).

As discussed by Stevens and Clemens (1993), fluid-absent anatexis is incompatible with the presence of a pervasive fluid, though fluid-present partial melting could occur with an H_2O–CO_2 fluid that had a sufficiently high $X^{Fl}_{H_2O}$. Regional carbonic metamorphism requires that the high-grade environment be pervasively flushed by CO_2-rich metasomatic fluid. Fluid-rock ratios must lie between 0.1 and 0.25 (Newton et al. 1980; Lamb and Valley 1984), to prevent buffering of the fluid composition by silicate dehydration equilibria.

Experiments indicate that carbonic fluid-mineral contacts are characterized by high dihedral angles (Watson and Brenan 1987; Holness and Graham 1991). Consequently, in a static environment, such fluids should form unreactive, isolated bubbles. This may account for the origin of common CO_2-rich fluid inclusions in granulite-grade migmatitic rocks, where other independent evidence indicates fluid-absent conditions. The CO_2 could be an externally derived retrograde fluid (e.g. Valley et al. 1990) or formed by local graphite ox-

idation (see below in the section on geological implications). Water-rich fluid inclusions can rapidly undergo hydrogen loss, producing inclusions with H_2O-poor compositions (Hall and Sterner 1993), and other mechanisms could also operate to change fluid inclusion compositions (e.g. Hollister 1988).

In contrast, fluid-absent anatexis is an unavoidable process at readily attainable crustal temperatures, provided that the crust is not permeated by a fluid with very low a_{H_2O}. This is believed to be the dominant mechanism of regional granulite formation. Carbonic fluid fluxing is probably limited to the vicinity of deformation zones that may allow fluid infiltration, as well as in direct proximity to crystallizing mantle-derived magmas and carbonate rocks undergoing devolatilization.

As suggested in the introduction, the above views of granulite formation have been challenged by some experimental data linking the presence of carbonic fluids with crustal anatexis at temperatures comparable to, or lower than, those at which hydrous silicates have been shown to break down in the fluid-absent environment. In the following sections, we establish the theoretical basis for discussing the experimental evidence, and then critically review and evaluate that evidence. We then describe new experiments designed accurately to map out the phase relations involving phlogopite-quartz breakdown in T–$X^{Fl}_{H_2O}$ space, to resolve any controversy over the role of CO_2 in high-grade metamorphism and crustal anatexis.

Theoretical analysis of phase relations in $KAlO_2$–MgO–SiO_2–H_2O–CO_2

As a preliminary tool for investigating the effects of CO_2-bearing fluids on the melting of biotite-quartz assemblages, we explore the phase relations of biotite, quartz and their potential breakdown products (K-feldspar, orthopyroxene, silicate melt, and a supercritical volatile-rich fluid phase) in simple Fe-free chemical systems, firstly with H_2O as the only volatile component, and then with CO_2 in addition.

K-AMSH system

The simplest chemical system in which end-members of the above phases can be described is the 4-component system $KAlO_2$–MgO–SiO_2–H_2O (K-AMSH). Phase relations in this system have been discussed by Luth (1967), Wones and Dodge (1977), Bohlen et al. (1983), Hewitt and Wones (1984), Grant (1985, 1986), Montana and Brearley (1989), Peterson and Newton (1989a), Vielzeuf and Clemens (1992) and Clemens (1995) and will be reviewed only briefly here. It is assumed that there is a miscibility gap between melt and fluid over the whole T range of interest (~750–950 °C), at crustal pressures. All phases can be considered to have fixed compositions in K-AMSH, except for the melt. The initial melt formed under H_2O-saturated conditions has a broadly "granitic" composition (e.g. Peterson and Newton 1989a; Clemens 1995) and plots very close to the Sa-Qtz join on a $KAlO_2$–MgO–SiO_2 (K-AMS) projection from H_2O (Fig. 1a). The melt field expands from a point to an area as T increases above the solidus.

The assemblage Phl + Qtz + En + Sa + M + Fl is invariant in K-AMSH, and can only exist in equilibrium at point I in Fig. 2. The six univariant equilibria that intersect at I are:

$$\text{Phl} + \text{Qtz} = \text{En} + \text{Sa} + \text{Fl} \quad [\text{M}]$$
$$\text{Phl} + \text{Sa} + \text{Qtz} + \text{Fl} = \text{M} \quad [\text{En}]$$
$$\text{En} + \text{Sa} + \text{Qtz} + \text{Fl} = \text{M} \quad [\text{Phl}]$$
$$\text{En} + \text{Sa} + \text{Fl} = \text{Phl} + \text{M} \quad [\text{Qtz}]$$
$$\text{Phl} + \text{Qtz} + \text{Fl} = \text{En} + \text{M} \quad [\text{Sa}]$$
$$\text{Phl} + \text{Qtz} = \text{En} + \text{Sa} + \text{M} \quad [\text{Fl}]$$

Here, the absent phase characterizing each reaction is given in brackets. The reaction relations of melt-bearing assemblages in K-AMSH depend critically on H_2O sol-

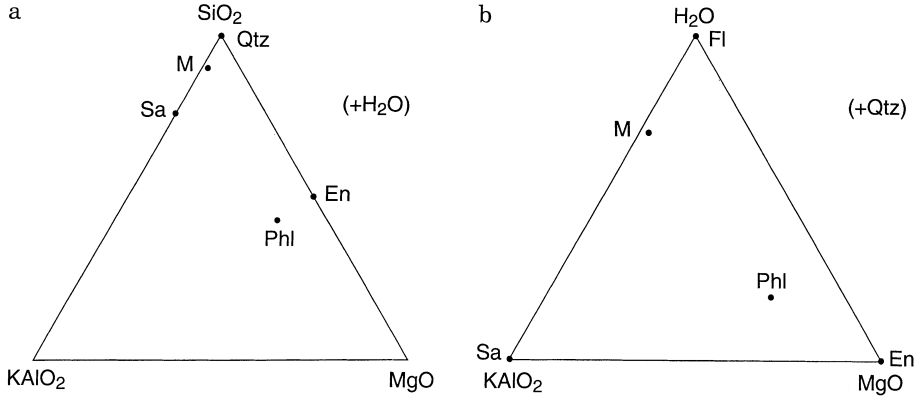

Fig. 1a,b Chemographic relations among the phases phlogopite (Phl), enstatite (En), sanidine (Sa), quartz (Qtz), melt (M) and fluid (Fl) in the system $KAlO_2$–MgO–SiO_2–H_2O (K-AMSH): **a** projected from H_2O onto the plane $KAlO_2$–MgO–SiO_2; **b** projected from SiO_2 onto the plane $KAlO_2$–MgO–H_2O. The composition of the melt is approximately that of the SiO_2- and H_2O-saturated melt in experiment K-107 (1.5 GPa, 725 °C) of Clemens (1995), though the MgO:$KAlO_2$ ratio has been exaggerated for clarity

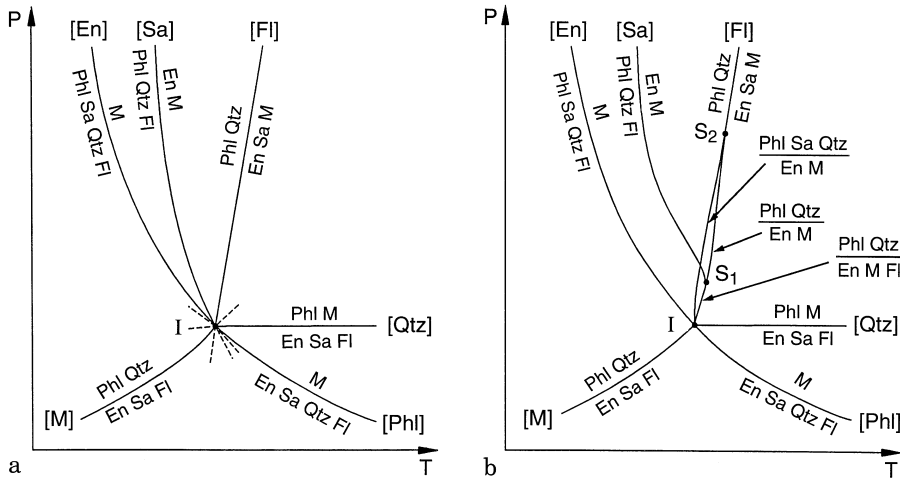

Fig. 2a,b Alternative topologies for the pressure-temperature petrogenetic grid involving reactions between phlogopite, orthoenstatite, high sanidine, quartz, silicate melt and aqueous fluid in the K-AMSH system. **a** Melts in the vicinity of the invariant point I are able to dissolve all the H_2O contained (as OH^-) in phlogopite. **b** Melts formed by incongruent melting reactions in the vicinity of I are unable to dissolve all the H_2O contained in phlogopite. See text for discussion

ubility in the melt. However, available experimental evidence (Luth 1967; Wones and Dodge 1977; Bohlen et al. 1983; Vielzeuf and Clemens 1992; Clemens 1995) places I at ~50 MPa and 820 °C and has demonstrated that the effective topology is as portrayed in Fig. 2 (see Clemens 1995). Thus, the key reactions limiting the stability of Phl-bearing assemblages at pressures corresponding to middle and lower crustal depths (~0.3–2 GPa) are [En], [Sa] and [Fl].

K-AMSHC system

In the K-AMSH system, described above, the reaction that limits the assemblage Phl + Qtz in the presence of fluid at $P > P_I$ is [Sa]. Whether CO_2 inhibits or enhances melting will thus depend on whether it is possible to generate a melting reaction involving H_2O–CO_2 fluid that is stable on the low-T side of [Sa]. Both previous experimental studies of this system (Wendlandt 1981; Peterson and Newton 1989b, 1990) imply that this *is* possible (see below).

The addition of the component CO_2 to the K-AMSH system will have the effect of increasing the variance of all the K-AMSH-univariant reactions by one, causing them to spread out into divariant fields. The six-phase assemblage, invariant in K-AMSH, will be drawn out to form a univariant reaction curve that terminates at I. Without the introduction of extra phases, this is the only new reaction that can appear on addition of CO_2, and its chemography and P–T position are therefore of paramount importance in this discussion. These factors are constrained by the relative solubilities of CO_2 in the six phases involved (Phl, En, Sa, Qtz, Fl and M). As CO_2 solubility in the crystalline phases is negligible, the only phases in which CO_2 can reside are melt and fluid, both of which are hydrous in K-AMSH. Thus, the K-AMSHC univariant curve is constrained to emerge from I somewhere in the segment occupied by the stability field of Phl + Qtz. (This is because incorporation of any CO_2 into the fluid phase will expand the stability field of En + Sa + Fl relative to Phl + Qtz, irrespective of the CO_2 content of the melt, resulting in the migration of reaction [M] to higher pressures. Similarly, incorporation of any CO_2 into the melt will cause expansion of the En + Sa + M field relative to Phl + Qtz, irrespective of fluid composition, resulting in the migration of curve [Fl] to lower temperatures.)

The chemography of the K-AMSHC univariant reaction and its P–T position depend entirely on the partitioning of CO_2 and H_2O between melt and fluid. Five theoretically possible alternatives are examined below, each involving a different degree of CO_2 partitioning. The chemographic relations are shown schematically on a MgO–H_2O–CO_2 projection from Sa and Qtz (Fig. 3a) and a $KAlO_2$–H_2O–CO_2 projection from En and Qtz (Fig. 3b). Fig. 4 shows the positions of the K-AMSHC univariant curves corresponding to each of these five alternatives. In Fig. 5, the phase relations, in up-T traverses across the P–T grid, at a pressure above I, are shown schematically as series of MgO–H_2O–CO_2 and $KAlO_2$–H_2O–CO_2 projections. The differences between these alternatives are illustrated further by means of isobaric temperature-H_2O activity (T–a_{H_2O}) diagrams (Fig. 6). The five alternatives are:

(a) Carbon dioxide soluble only in the fluid phase (i.e. $X^{M}_{CO_2} = 0$): In this limiting case the position of K-AMSH reaction [Fl] is unaffected by the addition of CO_2 to the system, so that the K-AMSHC univariant curve (U_1) is coincident with curve [Fl]. Any dilution of aqueous fluid by CO_2 would result in the deflection of *all* melting equilibria to higher T. However, this alternative is unrealistic, since small amounts of CO_2 are known to dissolve in all silicate melts (Carroll and Holloway 1994), and thus is not illustrated in Figs 5. and 6.

(b) where $X^{Fl}_{CO_2} >>> X^{M}_{CO_2} > 0$: In this case the composition of the melt involved in the K-AMSHC univariant reaction (M_2) is more H_2O-rich than the assemblages Phl + Sa + Qtz + Fl and Phl + En + Qtz + Fl. It therefore plots to the H_2O-rich side of the Phl + Fl tie-line in both projections in Fig. 3, and the univariant reaction is:

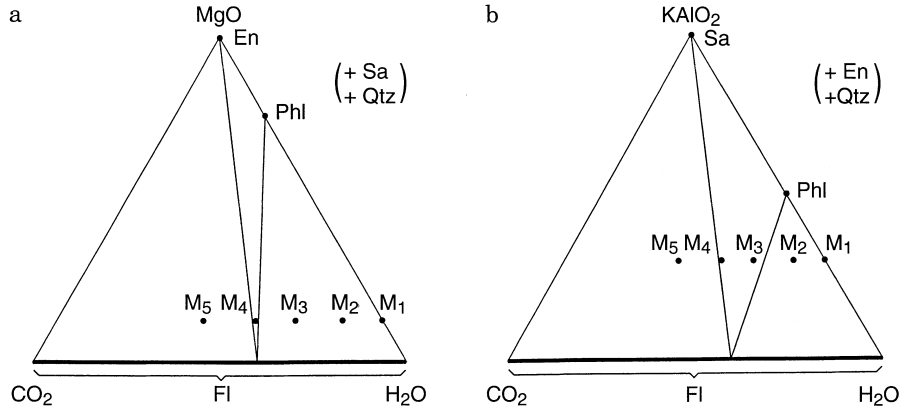

Fig. 3a,b Five possible alternatives for the partitioning of H_2O and CO_2 between melt and fluid, depicted schematically as five melt compositions (M_1, M_2, M_3, M_4 and M_5) coexisting with a fluid of given H_2O:CO_2 ratio on: **a** an MgO–CO_2–H_2O projection from sanidine and quartz; **b** a $KAlO_2$–CO_2–H_2O projection from enstatite and quartz. Melt composition M_1 contains no CO_2; M_2 plots on the high-H_2O side of the plane Phl-En-Fl in the quartz-saturated K-AMHC tetrahedron; M_3 plots between the Phl-Sa-Fl and Phl-En-Fl planes; M_4 plots between the En-Sa-Fl and Phl-Sa-Fl planes; M_5 plots on the high-CO_2 side of the plane En-Sa-Fl

$$\text{Phl} + \text{Qtz} + \text{Fl} = \text{En} + \text{Sa} + \text{M}_2 \qquad \text{U}_2$$

By Schreinemakers' rules (Zen 1966), the stable end of U_2 must extend from invariant point I, between the stable ends of K-AMSH curves [Fl] and [Sa]. Incorporation of small amounts of CO_2 into the melt expands

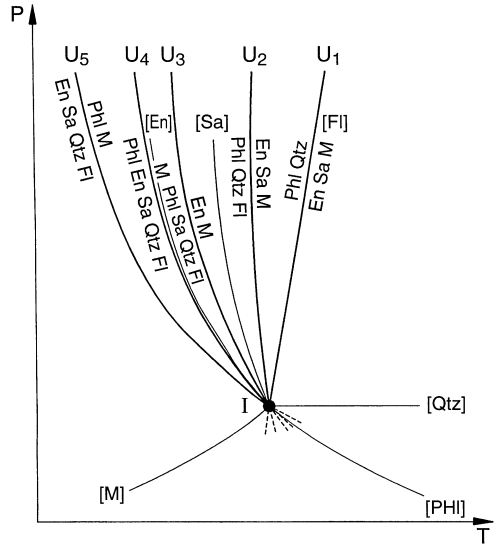

Fig. 4 Five possible locations (U_1, U_2, U_3, U_4 and U_5) for the univariant reaction involving the phases phlogopite (Phl), enstatite (En), sanidine (Sa), quartz (Qtz), melt (M) and fluid (Fl) in the $KAlO_2$–MgO–SiO_2–H_2O–CO_2 system (*bold curves*), in relation to the petrogenetic grid of Fig. 2(a) (*faint curves*). Location U_1 corresponds to M_1 of Fig. 4, U_2 to M_2, etc. Note that there is a one-to-one relationship between the topological position of the univariant curve and its reaction chemography (as dictated by Schreinemakers' rules: Zen 1966)

the stability fields of all melt-bearing assemblages relative to those in the first alternative. Thus, all melt-bearing reaction curves move to progressively lower T with decreasing a_{H_2O} or $X^{Fl}_{H_2O}$, in effect rotating about their respective intersection points with the vertical axis at $a_{H_2O} = 1$ (Fig. 6a). Only the melt-absent reaction curve [M] is unaffected by this. The point at which curves [Phl], [En], [Sa], [Qtz] and [M] intersect represents the K-AMSHC-univariant reaction which, in this case, is U_2. This point, U_2, is joined to point J by a sixth curve, that of the fluid-absent reaction [Fl]. The incorporation of small but variable amounts of CO_2 into the melt allows [Fl] to buffer a_{H_2O} over a range of values, from a maximum at J (representing CO_2-free melt coexisting with Phl, En, Sa and Qtz) to a minimum at U_2 (representing CO_2-saturation in the presence of Phl, En, Sa, Qtz and a binary H_2O–CO_2 fluid). Note that curves [En] and [Sa] both emerge on the low-T side of U_2, indicating deflection of all melting equilibria to higher T, with progressive enrichment of the system in CO_2.

(c) where $X^{Fl}_{CO_2} \gg X^{M}_{CO_2}$: In this case the composition of the melt involved in the K-AMSHC univariant reaction (M_3) is more H_2O-rich than the assemblage Phl + Sa + Qtz + Fl and more CO_2-rich than the assemblage Phl + En + Qtz + Fl, resulting in the following chemography for the univariant reaction:

$$\text{Phl} + \text{Sa} + \text{Qtz} + \text{Fl} = \text{En} + \text{M}_3 \qquad \text{U}_3$$

The stable extension of the U_3 curve must lie between those of [En] (the H_2O-saturated solidus in K-AMSH) and [Sa]. This is the chemography inferred by Wendlandt (1981) and Peterson and Newton (1990). The corresponding T–a_{H_2O} section is shown in Fig. 6, alternative (c). Here, T_{U_3}, the temperature of the K-AMSHC-univariant reaction (in this case U_3), is lower than T_3, the temperature of the K-AMSH end-member reaction [Sa]. Thus [M] and [En] are the only curves emerging from the low-T side of U, in keeping with the chemography of U_3. This means that, while the fluid-saturated congruent melting equilibria [En] and [Phl] are deflected to higher T with progressive addition of CO_2 to the system, the incongruent melting curve [Sa] moves to lower T. This alternative corresponds to the situation envisaged by Newton (1990); see Fig. 7.

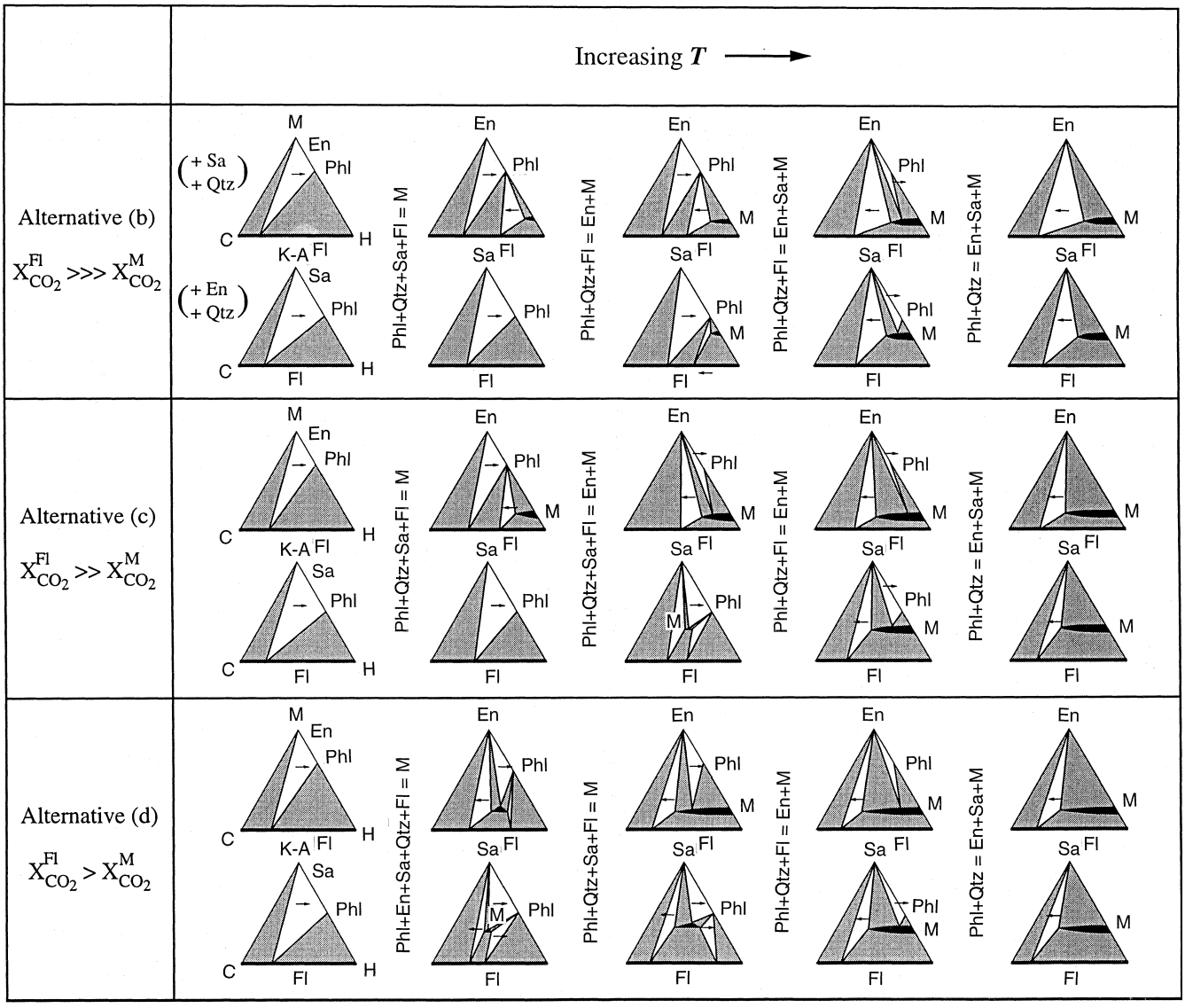

Fig. 5 Prograde reaction sequences at relatively high pressure (higher than point I in Fig. 2a) corresponding to the three plausible alternatives for H_2O–CO_2 partitioning between melt and fluid (see text for details). For each alternative, phase relations are shown on both MgO–CO_2–H_2O (M C H) projections from quartz and sanidine and $KAlO_2$–CO_2–H_2O (K-A C H) projections from quartz and enstatite. Complete immiscibility of melt and fluid is assumed. *Arrows* indicate migration directions of phase volumes in response to prograde continuous reactions. Note that, within each alternative, T increases to the *right*. However, since reactions occur in different orders for different alternatives, it is not possible to match T scales from one to another

(d) where $X^{Fl}_{CO_2} > X^{M}_{CO_2}$: In this case the composition of the melt involved in the K-AMSHC univariant reaction (M_4) is more H_2O-rich than the assemblage En + Sa + Qtz + Fl and more CO_2-rich than the assemblage Phl + Sa + Qtz + Fl, and so plots within the Phl + En + Fl and Phl + Sa + Fl triangles in Fig. 3a and b, respectively. The resultant K-AMSHC univariant reaction is:

$$\text{Phl} + \text{En} + \text{Sa} + \text{Qtz} + \text{Fl} = \text{M}_4 \qquad \text{U}_4$$

and is constrained to lie on the low-T side of the K-AMSH, H_2O-saturated solidus [En], but at higher T than the metastable extension of [Phl]. Here, T_{U_4} is lower than both T_2 and T_3 (Fig. 6c), so that both [En] and [Sa] melting curves are deflected to lower T with progressive addition of CO_2 to the system.

(e) where $X^{Fl}_{CO_2} < X^{M}_{CO_2}$: In this case the composition of the melt involved in the K-AMSHC univariant reaction (M_5) is more CO_2-rich than the assemblage En + Sa + Qtz + Fl and must plot to the left of the En + Fl and Sa + Fl tie-lines in Fig. 3a and b, respectively. The resultant K-AMSHC univariant reaction is:

$$\text{En} + \text{Sa} + \text{Qtz} + \text{Fl} = \text{Phl} + \text{M}_5 \qquad \text{U}_5.$$

This reaction implies prograde (up-T) growth of phlogopite by incongruent melting of an assemblage of anhydrous minerals and fluid. There is no geological or experimental evidence for such a reaction and, since all

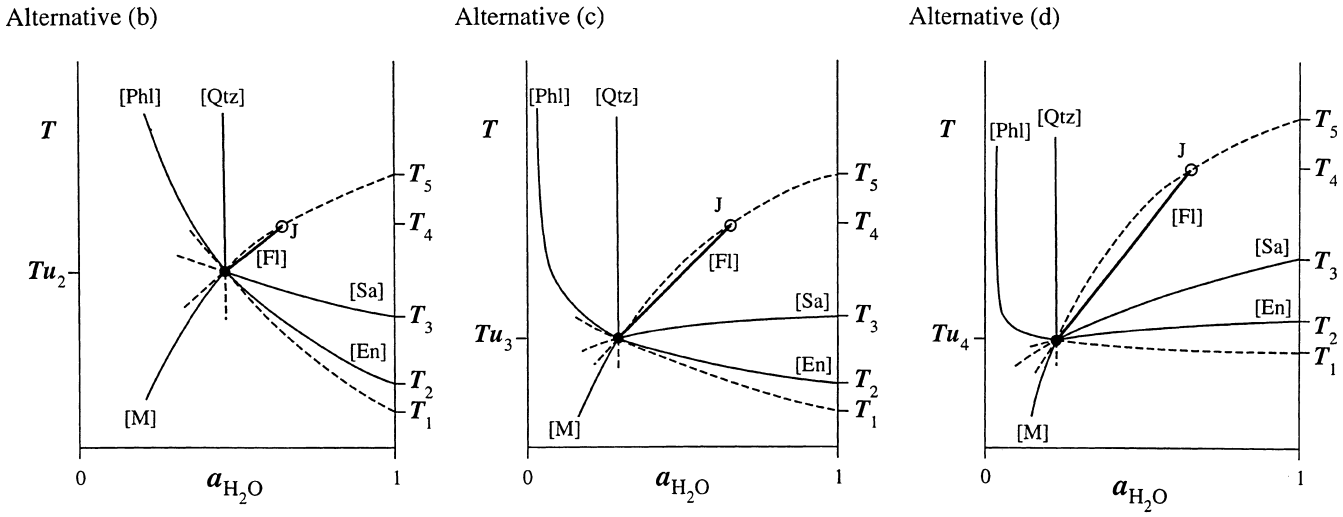

Fig. 6 Three schematic, isobaric, T-H_2O activity diagrams for equilibria in the K-AMSHC system, corresponding to the three plausible alternatives for H_2O–CO_2 partitioning between melt and fluid, as depicted in Figs. 3, 4 and 5. (**b**) $X^{Fl}_{CO_2} >>> X^{M}_{CO_2}$; (**c**) $X^{Fl}_{CO_2} \gg X^{M}_{CO_2}$; (**d**) $X^{Fl}_{CO_2} > X^{M}_{CO_2}$. T_1, T_2, T_3, T_4 and T_5 are the equilibrium temperatures for univariant K-AMSH reactions [Phl], [En], [Sa], [Fl] and [M] (metastable in the case of [Phl] and [M]) at an arbitrary constant pressure above I in Fig. 2(a). J is the T-a_{H_2O} point that corresponds to K-AMSH reaction [Fl] and, like $T_1 \ldots T_5$, is the same in all five alternatives. U is the T-a_{H_2O} point that corresponds to the K-AMSHC univariant reaction, and involves a CO_2-saturated melt that coexists with Phl, En, Sa, Qtz and a binary H_2O–CO_2 fluid. In each case, U is joined to J by a reaction curve that represents the fluid-absent reaction in which the melt contains finite, but non-saturating, amounts of CO_2 (Phl + Qtz = En + Sa + M). Note that, progressing from (**b**) to (**d**), the number of curves with positive dT/da_{H_2O} slopes increases, indicating increasing stabilization of reactions by the addition of CO_2. CO_2-induced depression of Phl + Qtz melting temperatures obtains where the K-AMSHC divariant reaction (Sa) has a positive slope, i.e. in alternatives (**c**) and (**d**). These diagrams can be converted readily to isobaric temperature-fluid composition (T-$X^{Fl}_{H_2O}$) diagrams by deleting the fluid-absent portions

experimental evidence has shown that CO_2 partitions preferentially into any fluid coexisting with a silicate melt, this alternative is implausible. It is not illustrated in Figs. 5 and 6.

Having dealt with the theoretical considerations, we now turn our attention to the experimental evidence, to decide which of the three plausible alternatives, (b), (c) or (d), operates in nature, and therefore which type of behaviour to expect during metamorphism in the presence of an H_2O–CO_2 fluid phase. First we examine the meaning of previous experimental studies in K-AMSHC, and then present the results of our own work.

Discussion and evaluation of previous experimental work

Clemens (1981)

Clemens' Ph.D. thesis contains the results of a series of 500 MPa experiments on various reactions in the system. Though previously unpublished, the results are briefly described here, to provide an historical perspective. Complete experimental details are given below in the section dealing with the present experiments, where the mineral mixes used (Table 1, Fig. 8) are fully described. Graphite precipitation in two low-T experiments necessitated calculation of the true $X^{Fl}_{H_2O}$ (see Appendix).

The position of the subsolidus reaction [M] was constrained in T–$X^{Fl}_{H_2O}$ space and reversed at one temperature. The solidus (reactions [Phl] and [En]) was approximately located and the position of the fluid-saturated reaction [Sa] was constrained. Results are presented as part of Table 2, and discussed later.

Wendlandt (1981)

The experiments of Wendlandt (1981) do not constrain the equilibria with which we are concerned. However, reactions involving phlogopite-quartz breakdown in the presence of H_2O–CO_2 fluids have been discussed in relation to the genesis of charnockites and granulites (see, e.g. Grant 1986); interpretations of Wendlandt's results form the basis for these ideas.

Starting material W (Fig. 8) was synthesized from a gel. It contains excess sanidine component and, as Wendlandt recognized, can strictly be used only to delineate the fluid-saturated solidus [En], *not* the fluid-present phlogopite + quartz melting reaction [Sa] or the isobarically invariant reaction (U). Interpretation of the results is further complicated by the fact that W also contains excess enstatite component (apparently unrecognized by Wendlandt).

It is important to note that the ludox sol, used in the gel preparation, introduced some Na contamination into the system. Wendlandt and Eggler (1980a) give a partial analysis of their phlogopite gel. From this we calculate that their synthetic "phlogopite" must have contained ~2.6 mol% of sodic mica solid solution. All other phases would have contributed Na to the mixtures also.

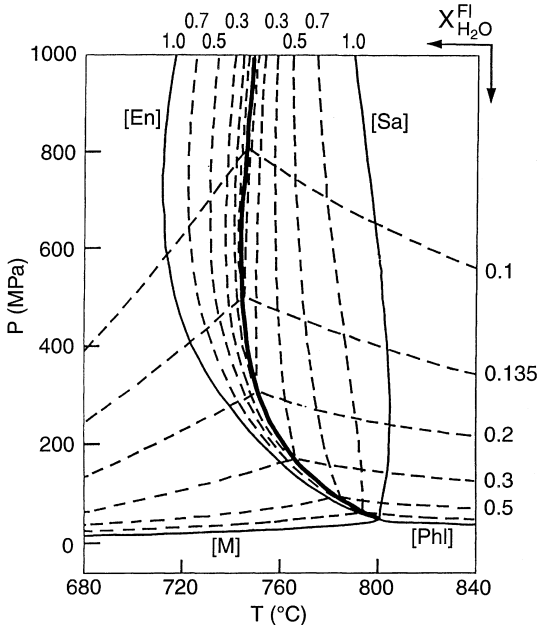

Fig. 7 *P-T* plot redrafted from Fig. 7.6 of Newton (1990). The plot shows Newton's interpretation of the locations of reactions [M], [Phl], [En] and [Sa] in the system $KAlO_2-MgO-SiO_2-H_2O$, as well as his views on how the loci of these equilibria shift in response to changes in $X^{Fl}_{H_2O}$ when CO_2 is introduced as a component in the system. Note that the diagram shows [M], [Phl] and [En] all shifting to higher T as $X^{Fl}_{H_2O}$ decreases (increased CO_2 content). However, reaction [Sa] is depicted shifting to lower T, enlarging the melt field, as $X^{Fl}_{H_2O}$ decreases. This corresponds to alternative (c) in our theoretical analysis, and implies a higher solubility of CO_2 in the melt than in the coexisting fluid. This notion is at odds with all experimental evidence on fluid-melt partitioning. Also note that the shapes and locations of the curves for [Sa] bear little resemblance to those determined in previous and subsequent experimental investigations. The thicker solid curve represents the supposed location of the univariant reaction Phl + Qtz + Fl = En + Sa + M in the system $KAlO_2-MgO-SiO_2-H_2O-CO_2$. See also Fig. 12

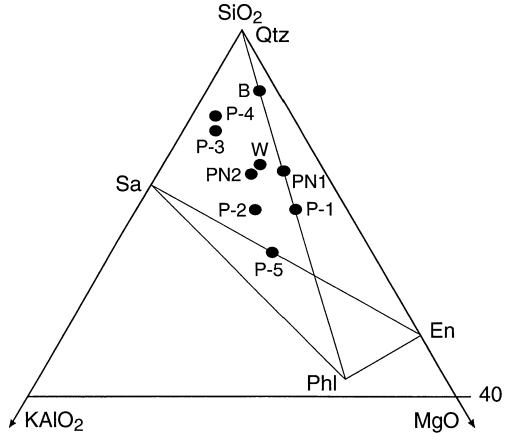

Fig. 8 *Upper* portion of a triangular plot of molar SiO_2–$KAlO_2$–MgO, showing the compositions of the starting materials used in the present and previous experimental studies of the system. All compositions are shown projected from H_2O

Table 1 Compositions (wt%) of mineral mixes used in the experiments

Mineral phase	P-1	P-2	P-3	P-4	P-5
Phlogopite	50	0	10	0	0
Enstatite	0	36.4	0	5	35
Quartz	50	30	45.5	47.5	0
Sanidine	0	33.6	45.5	47.5	65

Thus we calculate that up to 2.5 wt% Na_2O may have been present in composition W. Since the "phlogopite" gel was also alkali deficient, the synthetic product would actually have been a slightly sodic solid solution of phlogopite-eastonite plus a small amount of excess enstatite. Wendlandt (1981, p. 1168) notes the presence of enstatite, coexisting stably with phlogopite, in the products of subsolidus runs on composition W. Samples were encapsulated with $Ag_2C_2O_4$ (as a source of CO_2) or with $H_2C_2O_4.2H_2O$ (as a source of a mixed H_2O–CO_2 fluid). No reversals were attempted.

As expected, all runs at $T < 1000$ °C (300 and 800 MPa) with $X^{Fl}_{CO_2} \approx 1$ resulted in subsolidus dehydration, the products being mixtures of quartz, sanidine, enstatite and CO_2-rich fluid. With an H_2O–CO_2 fluid phase initially present, the solidus reaction [En] was located between 747 and 778 °C at 300 MPa and 1.5 GPa, and between 722 and 753 °C at 800 MPa. This is seriously inconsistent with the Bohlen et al. (1983) experiments on the solidus in the MgO-free analogue system (K-ASHC), and with the present experimental data (see later). If $X^{Fl}_{H_2O}$ had really been 0.5, the solidus should have been found at temperatures at least 50 °C higher. The location given by Wendlandt (1981) would be consistent with experiments at $X^{Fl}_{H_2O} \approx 0.7$.

Wendlandt used fluid:solid or melt ratios of ≤ 0.1, with sample masses of about 0.01 g. The phlogopite-bearing starting mixture contained 0.55 wt% H_2O. We calculate that the theoretical $X^{Fl}_{H_2O}$ would thus have been between 0.54 and 0.57. This calculation assumes:(1) that the oxalic acid dihydrate would decompose to give equimolal quantities of H_2O and CO_2; (2) decomposition of ≥90% of the phlogopite, (3) that between 5 and 10 wt% of each sample was fluid; (4) that initial solid sample masses were 0.01 g. The first assumption may be invalid. Oxalic acid dihydrate is somewhat hygroscopic, and there is no mention of standardization of this reagent for its H_2O and CO_2 yields. Additionally, the Na contamination in the starting materials would have caused a lowering of the solidus (relative to the Na-free system). These cumulative effects probably explain the anomalously low T of the solidus at $X^{Fl}_{H_2O}$ = "0.5".

On the basis of topological considerations, and the experimental data of Wendlandt and Eggler (1980b), Wendlandt (1981) predicted that H_2O-undersaturated melts in this system would become less silicic and more potassic and magnesian with decreasing a_{H_2O} (and increasing T). This idea was taken up by Peterson and

Table 2 Experimental results: results at $X^{Fl}_{H_2O} = 1$ (from Clemens 1995) are included here to provide a complete data set, from which T-$X^{Fl}_{H_2O}$ sections can be constructed

Run no.	P (MPa)	T (°C)	$X^{Fl}_{H_2O}$	Duration (h)	Starting material	Assemblage
[M]						
K-135[a]	504	717 ± 6	0.10[a]	240	P-1	Phl, Qtz, graphite[f]
K-136[a]	504	717 ± 6	0.10[a]	240	P-5	Phl, Qtz, graphite[f]
K-119[a]	504	807 ± 16	0.10	215	P-1	(Phl), (Qtz), En, Sa
K-120[a]	504	807 ± 16	0.10	215	P-5	(Qtz), En, Sa
K-121[a]	504	807 ± 16	0.20	215	P-1	(Phl), (Qtz), En, Sa
K-122[a]	504	807 ± 16	0.20	215	P-5	(Phl), (Qtz), En, Sa
K-123[a]	504	807 ± 16	0.30	215	P-1	(Phl), (Qtz), En, Sa
K-124[a]	504	807 ± 16	0.30	215	P-5	(Phl), (Qtz), En, Sa
K-125[a]	504	807 ± 16	0.40	215	P-1	Phl, Qtz, (En), ((Sa))
K-126[a]	504	807 ± 16	0.40	215	P-5	Phl, Qtz, (En), (Sa)
K-70	1017	800 ± 1	0.33	144	P-1	Phl, Qtz, En, Sa
K-75	1003	800 ± 1	0.35	146	P-5	Phl, Qtz, (Sa)
K-72	1011	800 ± 1	0.35	142	P-1	Phl, Qtz
K-109	1498 ± 8	850 ± 1	0.33''	147	P-1	Qtz, En, Sa, Gl, graphite
[En]						
K-106	506 ± 1	809 ± 1	0.52	161	P-3	(Phl), Qtz, Sa
K-114	506 ± 2	710 ± 1	1.00	163	P-3	(Phl), Qtz, Sa
K-92	1003 ± 8	850 ± 1	0.43	97	P-4	(Phl), Qtz, (En), Sa, (Gl) (on invariant point)
K-89	1011 ± 15	835 ± 1	0.45	97	P-3	(Phl), En, Gl
K-95	1000 ± 10	820 ± 1	0.47	8	P-3	(Phl), Qtz, Sa
K-87	995 ± 28	770 ± 1	0.71	98	P-3	(Phl), Qtz, Sa
K-84	1028 ± 28	780 ± 1	0.72	97	P-3	(Phl), Qtz, (Sa), Gl
K-83	1000 ± 20	790 ± 1	0.68	130	P-3	(Phl), Qtz, Gl
K-79	1015 ± 14	710 ± 1	1.00	124	P-3	(Phl), Qtz, Sa
K-81	1011 ± 24	720 ± 1	1.00	97	P-3	(Phl), Qtz, Sa, (Gl)
K-107	1499 ± 7	725 ± 1	1.00	122	P-3	(Phl), ((Qtz)), Sa, Gl
[Phl]						
K-116	502 ± 1	942 ± 2	0.19	50	P-4	(Qtz), (En), Gl
K-93	1002 ± 16	1025 ± 1	0.05	49	P-4	Qtz, (En), Gl
K-91	996 ± 5	1045 ± 1	0.05	47	P-4	Qtz, (En), Gl
K-96	1004 ± 13	1000 ± 1	0.07	48	P-4	Qtz, (En), Sa
K-71	998 ± 28	930 ± 1	0.22	9	P-4	Qtz, (En), Gl
K-94	995 ± 10	890 ± 1	0.27	72	P-4	Qtz, (En), Gl (Na contamination?)
K-97	1008 ± 4	880 ± 1	0.29	72	P-4	Qtz, (En), Sa
K-99	1000 ± 10	890 ± 1	0.30	0.2	P-4	Qtz, (En), Sa
K-98	1003 ± 10	850 ± 1	0.38	97	P-4	Qtz, (En), Sa
K-90	1002 ± 11	870 ± 1	0.40	100	P-4	Qtz, Gl
K-88	986 ± 7	880 ± 1	0.40	3	P-4	Gl (possible failure)

Newton (1989b, 1990), whose reported experimental data appeared to support this, even to the production of highly magnesian, silica-poor ''lamprophyric'' melts. Analyses of glasses formed in our own experiments (also see Clemens 1993) lend no support to this prediction (see below).

Bohlen, Boettcher, Wall and Clemens (1983)

The Bohlen et al. (1983) phlogopite was prepared from K_2CO_3, MgO, Al_2O_3 and SiO_2, reacted hydrothermally. Brazilian quartz was finely ground, leached in HNO_3 and fired at 800 °C for 48 h. Sources of H_2O and CO_2 were boiled, doubly distilled, deionized water and standardized $Ag_2C_2O_4$. The experimental apparatus was a 1.27 cm piston cylinder used with NaCl pressure cells and graphite tube furnaces. Calibration methods were detailed in Bohlen and Boettcher (1982) and we estimate P and T uncertainties to have been about ±20 MPa and ±3 °C.

Actual starting materials were mixtures of phlogopite, quartz, enstatite and sanidine (1:3:3:1 mole ratio) for reversal of subsolidus reaction [M]. This composition is plotted as B in Fig. 8. Bohlen et al. report a thermal reversal of [M] at high P. At 500 ± 20 MPa and $X^{Fl}_{H_2O} = 0.35$, the reaction lies between 780 and 800 ± 3 °C. This approximately agrees with Clemens' (1981) reversal in $X^{Fl}_{H_2O}$; at 503.9 ± 4 MPa and 807 ± 16 °C, the reaction lies between $X^{Fl}_{H_2O} = 0.3$ and 0.4.

Table 2 (continued)

Run no.	P (MPa)	T (°C)	$X^{Fl}_{H_2O}$	Duration (h)	Starting material	Assemblage
Mostly [Sa]						
K-100	347 ± 2	772 ± 1	0.50[b]	287	P-1	Phl, Qtz
K-101	347 ± 2	772 ± 1	0.50[c]	287	P-1	Phl, Qtz
K-104	342 ± 1	784 ± 1	0.50[d]	112	P-1	Phl, Qtz
K-105	342 ± 1	784 ± 1	0.30[e]	112	P-2	(Phl), Qtz, En, Sa
K-117[a]	504 ± 4	807 ± 16	0.60	215	P-1	Phl, Qtz
K-102	506 ± 1	809 ± 1	0.75	161	P-1	Phl, Qtz
K-118[a]	504 ± 4	807 ± 16	1.00	215	P-1	Phl, Qtz
K-103	506 ± 1	809 ± 1	1.00	161	P-1	Phl, Qtz
K-115	503 ± 1	836 ± 2	1.00	118	P-1	(Phl), En, Gl
K-80	1003 ± 23	810 ± 1	0.71	96	P-1	Phl, Qtz
K-82	1004 ± 11	820 ± 1	0.71	105	P-1	(Qtz), En, Gl
K-76	1007 ± 25	740 ± 1	1.00	119	P-1	Phl, Qtz
K-78	1003 ± 24	750 ± 1	1.00	111	P-1	Phl, Qtz
K-74	1010 ± 33	760 ± 1	1.00	122	P-1	Phl, Qtz, En, Gl
K-68	996 ± 36	765 ± 1	1.00	122	P-1	Phl, Qtz, En, Gl
K-67	1001 ± 37	770 ± 1	1.00	96	P-1	Phl, Qtz, (En), (Gl?)
K-42	1000 ± 22	775 ± 1	1.00	85	P-1	Phl, Qtz, ((En))
K-5	1010 ± 20	780 ± 1	1.00	159	P-1	Phl, Qtz, (En), (Gl)
K-108	1501 ± 15	840 ± 1	0.70	97	P-1	(Phl), (Qtz), En, Gl
K-77	1524 ± 21	785 ± 1	1.00	47	P-1	Phl, Qtz, En, (Gl)

[a] Run result from Clemens (1981)
[b] Oxalic acid dihydrate, $f_{H_2} = 6.2$ MPa (duplication of Peterson and Newton run 260)
[c] $H_2O + Ag_2C_2O_4$, $f_{H_2} = 6.2$ MPa
[d] Oxalic acid dihydrate, $f_{H_2} = 6.5$ MPa (duplication of Peterson and Newton, (1990, run 254)
[e] Duplication of K-104 but with Qtz + En + Sa starting mix
[f] For calculation of $X^{Fl}_{H_2O}$ in these runs, see Appendix

Peterson and Newton (1989b, 1990)

These experiments used synthetic phlogopite and sanidine, and natural quartz. The actual starting materials were mixtures of phlogopite + quartz (2:3 mass ratio) and phlogopite + sanidine + quartz (2:2:3 mass ratio), plotted as PN1 and PN2 in Fig. 8. Platinum capsules were loaded with the starting mixes and varying amounts of $H_2C_2O_4$ and $H_2C_2O_4.2H_2O$, to generate $X^{Fl}_{H_2O}$ between "0.0" and 0.5. Runs were carried out in internally heated vessels and a piston cylinder apparatus with NaCl cells. Though some low-T runs resulted in graphite precipitation, final $X^{Fl}_{H_2O}$ compositions were determined by thermogravimetry.

Data were collected on [Sa] at 200 to 600 MPa and $X^{Fl}_{H_2O} \approx 0.5$, with a reversal reported at 350 MPa. Melting apparently occurred at T as low as 763 °C at 600 MPa. For [En], experiments with $X^{Fl}_{H_2O} \approx 0.5$ were performed at 200 MPa to 1 GPa. However, no brackets or reversals were obtained. Signs of melting were recorded at T as low as 671 °C, at 1 GPa. At 250 MPa, they report experiments that appear to constrain the position of the univariant reaction (U) to between 757 and 782 °C. This is at only slightly higher T than the solidus [En] determined for $X^{Fl}_{H_2O} = 1$ (Clemens 1995), yet the Peterson and Newton experiments were carried out with $X^{Fl}_{H_2O}$ between 0.1 and 0.41.

As indicated above, Peterson and Newton reported melting, in the presence of CO_2–H_2O fluids, at temperatures more than 50 °C below the modelled solidus at $X^{Fl}_{H_2O} < 1$, and CO_2-enhanced melting at temperatures as much as 30 °C below the experimentally determined H_2O-saturated solidus. These workers postulated the existence of thermal minima on [En] and [Sa], in T-$X^{Fl}_{H_2O}$ space (see Fig. 9). If correct, this would require that CO_2

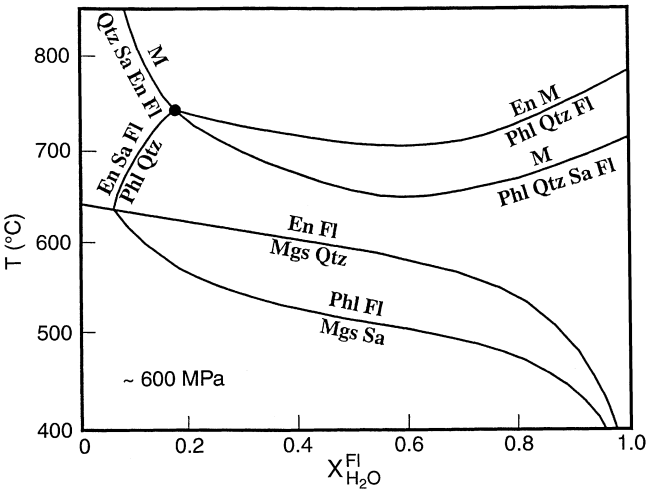

Fig. 9 Redrawn and simplified version of Fig. 8 of Peterson and Newton (1990). The diagram shows these authors' interpretation of isobaric phase relations in T-$X^{Fl}_{H_2O}$ section at a pressure of about 600 MPa. The two equilibria involving magnesite (Mgs) can be ignored for the present discussion. The *large dot* is the isobaric invariant point at which phlogopite, quartz, enstatite, sanidine, melt and fluid all coexist. The major feature to note is that reactions [En] and [Sa] are both shown passing through thermal minima at $X^{Fl}_{H_2O} \approx 0.6$, consistent with Peterson and Newton's inference that the presence of CO_2 in the fluid phase can cause crustal melting to occur at temperatures lower than for pure H_2O fluid

be more soluble than H_2O in the melts at the same *P-T* conditions and the chemography and topology of the system would be that for alternative (e) above (see also Fig. 7). However, experiments on a wide range of melt compositions (silicic to mafic and alkaline, silica-undersaturated) have shown that CO_2 solubility is 10 to 1,000 times lower than that of H_2O at any given experimental conditions (e.g. Mysen et al. 1975; Eggler and Kadik 1979; Holloway and Jakobsson 1986; Fogel and Rutherford 1990; Holloway et al. 1992; Pawley et al. 1992; Blank et al. 1993). We will further discuss the results of Peterson and Newton following the description of our own experimental data.

Clemens (1993)

The reports, by Peterson and Newton (1989b, 1990), of CO_2-fluxed melting and the formation of highly magnesian (''lamprophyric'') melts in the system, spurred Clemens (1993) to carry out experiments specifically designed to duplicate the run conditions of those previous workers.

Clemens used the same type of apparatus and platinum capsules, with standardized oxalic acid dihydrate to generate H_2O–CO_2 fluids with $X^{Fl}_{H_2O} = 0.5$. The starting material was P-1 (see Table 1). In all respects, the experimental conditions were as similar as possible to those reported by Peterson and Newton (1990) for their runs 254 and 260. These two runs were chosen for duplication because they were reported to have produced melt (quenchable to a glass), with near elimination of phlogopite and formation of abundant enstatite crystals. Also, the glass from run 254 had been analysed and is typical of Peterson and Newton's low-SiO_2, high-MgO material.

The results of Clemens (1993) are reiterated in Table 2; they did not confirm the results of Peterson and Newton. Both sets of runs (K-100 and K-104/K-105) were clearly at subsolidus conditions; no reaction took place in either K-100 or K-104. Furthermore, in run K-105 which used starting material P-5, growth of phlogopite was verified by optical, X-ray diffraction and SEM examinations. This confirmed that phlogopite + quartz is the stable assemblage at these run conditions.

Present experiments

Apparatus

Experiments at $P \leq 200$ MPa: most of the lower-pressure experiments were run (at Clermont-Ferrand) in cold-seal vessels, with vertically mounted furnaces and N_2 as the pressure medium. Temperatures were measured with external, type-S thermocouples and are believed accurate to ± 2 °C. Thermal gradients were measured with an internal, type-K thermocouple at 1 atm and 800 °C. These amounted to < 1 °C over 2 cm at the sample locations in the vessels. Pressure was monitored using a solid-state transducer accurate to ± 0.6 MPa. Week-long runs, at 100 MPa and 800 °C, with Pt capsules containing various metal-oxide-H_2O systems, showed that the intrinsic f_{O_2}/f_{H_2} of the system is close to $Fe_3O_4 + Fe_2O_3 + H_2O$ or $Cu + Cu_2O + H_2O$.

Experiments at 500 MPa: all 500 MPa experiments were carried out in the large-volume, internally heated vessels, formerly in the Department of Earth Sciences at Monash University, in Australia. The vessels were run vertically and are similar to those described by Burnham (1962). The pressure medium was Ar and the samples were heated by two-zone, inconel, resistance furnaces. Pressure was measured by a manganin resistance cell, itself calibrated against a 0–700 MPa Heise gauge. Temperatures were monitored by type-K thermocouples calibrated against a type-S, standard thermocouple (itself calibrated by the National Measurement Laboratory, C.S.I.R.O., Australia). Reported temperatures are accurate to ± 2 °C. All runs were carried out with f_{H_2} imposed by an H_2 diffusion membrane of $Pd_{60}Ag_{40}$. Oxygen fugacity was 1.3 (± 1) log units below FMQ, as calibrated by O'Neill (1987).

Experiments at $P \geq 1$ GPa: all higher-pressure experiments were carried out in end-loaded and non-end-loaded piston-cylinder vessels at Manchester University. Pressure cells were NaCl-MgO, with graphite furnace tubes. Temperatures were measured with type-R, Pt-Rh thermocouples. Thermal gradients of ~2 °C across the 0.6 mm-thick samples are estimated from the measurements of Esperança and Holloway (1986) and Jakobsson and Holloway (1986), on similar types of sample assembly. Reported temperatures are considered accurate to ± 2 °C.

Starting materials

Phlogopite

Two batches of hydroxyphlogopite were synthesized. The first (used by Clemens, 1981) was made from a mixture of $K_2O.3SiO_2$ glass plus MgO, Al_2O_3 and excess H_2O. The potassium silicate glass was made by 1 atm fusion (at 750 °C) of a mixture of K_2CO_3 and pure SiO_2 glass. Clemens (1995) gives details of the provenance, treatment and storage of all reagents used in the syntheses. The phlogopite was synthesized in a 300 h run at 360 MPa and 700 °C. Optical and X-ray examination showed the product to be pure, very fine grained, *1M* or *3T* phlogopite. This material was used in starting mixes for the 500 MPa experiments. A second batch was synthesized from $KAlSi_3O_8$ gel plus MgO and excess H_2O. Vielzeuf and Clemens (1992) contains all details of this mica, which was used in all other experiments.

Sanidine

Details of the pure high sanidine used are given by Clemens (1995).

Enstatite

For the 500 MPa experiments, pure orthoenstatite was synthesized from a mixture of MgO and SiO_2 glass, reacted with excess H_2O at 300 MPa and 800 °C for 120 h. For all other experiments the enstatite was synthesized from a gel plus excess H_2O; details are given in Clemens (1995).

Quartz

All quartz used in here was finely ground (−10 μm), acid washed, Brazilian, optical grade, rock crystal.

Starting mineral mixtures

Several different mineral mixtures were used as starting materials. Table 1 shows their compositions, which are plotted in Fig. 8 also. Most were made by grinding the pure, synthetic materials (+ quartz) together, in a mechanical agate mortar, under acetone, for 20 min. Mixture P-5 was made by gentle, hand grinding in an agate mortar, to avoid quartz contamination. All mixes were dried at 110 °C and stored in vacuum desiccators, over silica gel.

Mixes 1 and 2 were used as the starting materials for Clemens' (1981) 500 MPa reversal of subsolidus dehydration reaction [M]. These consist of 93% reactants, 5% products and 2% excess quartz. Mix P-1 was the starting material for investigating reactions [M] and [Sa] at low P and for all 1.0 and 1.5 GPa experiments. It was also used, along with P-2, for the special runs designed to duplicate the conditions of Peterson and Newton (1989b, 1990). Mix P-3 was used in experiments on [En], P-4 on [En] and [Phl], and P-5 on [M] at pressures other than 500 MPa.

Experimental techniques

For experiments at $P \leq 200$ MPa, thin-walled Pt capsules were loaded with about 0.02 g of starting material. Carefully measured amounts of H_2O and $Ag_2C_2O_4$ were added, and the capsules sealed by carbon arc welding.

For 500 MPa experiments, the capsules were $Pd_{50}Ag_{50}$ or $Pd_{30}Ag_{70}$ and sample masses were 0.015 to 0.02 g. A predetermined mass of silver oxalate was weighed into the capsule. This was topped with the sample and the required mass of water was added before sealing. Quantities of silver oxalate and H_2O were calculated so that the capsules would be ~80% filled at run P and T, with the mass ratio solid ± melt:fluid ≥ 1. End-of-run fluid compositions were checked by thermogravimetry and found to be generally within ±3% of the desired $X^{Fl}_{H_2O}$. Values reported for $X^{Fl}_{H_2O}$ are those derived from the quantities of silver oxalate and water loaded (measured to ±0.0001 g) and corrected for the adsorbed H_2O in the $Ag_2C_2O_4$.

In the experiments at higher P, approximately 0.02 g of starting material was loaded into small Pt capsules. Silver oxalate and H_2O were added in a similar manner and the capsules sealed. In all cases the capsules were then squashed flat and folded into "packets" with approximate dimensions of $3.5 \times 5 \times 0.6$ mm. These packets lay flat in the pressure cells so that the samples would experience the minimum possible thermal gradients.

All experiments were simultaneously brought to final P-T conditions, and the hot piston-out technique was used for the piston-cylinder runs. Experimental conditions were monitored and recorded several times per day, over the course of each run. Reported temperatures are the averages of the recorded minima and maxima, and quoted uncertainties represent the total ranges of temperature variation during the runs. A similar procedure was followed for the pressure measurements. To avoid vesiculation of volatile-bearing glasses, all experiments were quenched isobarically. Quench rates were of the order of 100 °C/s in the piston cylinder, 3 °C/s in the cold-seal vessels (cooled by air jet) and 1 °C/s in the internally heated vessels.

After the runs, the survival of the capsules was checked by comparing post- with pre-run masses. The results for capsules showing significant mass loss were disregarded.

Observation and analysis of run products

The contents of each capsule were split into several portions. Part was ground under acetone and used to make an optical grain mount. Microscopic examination of these grain mounts was the principal method of phase identification.

X-ray powder diffractometry was used to detect sanidine, since optical identification was difficult. Both CGR and Siemens type-F diffractometers were used, with Cu Kα radiation, and 2θ-D relations were calibrated against Au and quartz internal standards.

Electron probe analysis of run products was carried out on the Manchester University JEOL JSM 6400 SEM, fitted with a Link EXL EDS analytical system and an Oxford Instruments cryo-stage. The accelerating potential was 15 kV and the probe current was 1.5 nA. Specimens were carbon coated and counting times varied from 40 to 100 s real time. We used ZAF4 software for the data processing. The reader is referred to Vielzeuf and Clemens (1992) for details of the use of the cryo-stage during analysis of light elements in the quench glasses.

Identification and description of phases in run products

Phlogopite

In all experimental run products, phlogopite mostly forms very fine grained masses in which individual crystals are difficult to distinguish. However, there are usually a few crystals that attain a substantial size (≤ 10 μm). These larger grains are colourless and have medium relief (that varies with crystal orientation), high birefringence and straight extinction.

Quartz

This phase always occurs as subhedral to anhedral grains of low relief and low birefringence. In all super-solidus runs, quartz grains are commonly larger (≤ 25 μm) than in the starting material. The larger grains have rounded, subhedral β habit.

Enstatite

High-relief needles and prisms with straight extinction and very low birefringence characterize this phase, but the forms of enstatite crystals vary. Very elongate, needle-like crystals are the norm (length/width averaging about 8). In super-solidus runs at 1 GPa, these needles attain lengths of up to 1 mm. They were generally much smaller in low-P runs and runs without significant quantities of glass (quenched melt). At low pressures (≤ 200 MPa) some of the crystals usually have markedly inclined extinction, indicating metastable formation of clinoenstatite.

Sanidine

This phase was not usually identified optically but its presence was detected through characteristic X-ray reflections (corresponding to $\bar{2}01$, 130, $\bar{2}02$ 002, 131 and 060 planes). This K-feldspar is always in the high structural state, as confirmed by the methods of Wright (1968).

Glass (quenched melt)

In runs at $P \geq 500$ MPa, colourless, isotropic glass was easily recognized. At lower pressures, glass was not always readily identifiable by optical means. Its presence was inferred from the coherency, brittleness and hardness of the run products when they were being crushed in an agate mortar. Our previous experience with similar experimental systems suggests that this method is both sensitive and reliable, allowing detection of as little as 5% glass in a run product. In some cases, powder XRD patterns also showed a glass "hump". The difficulty of identifying glass results from the

small extents of reaction, due to the extreme sluggishness of phlogopite breakdown at $P < 500$ MPa and $T < 800$ °C (see Clemens 1995).

Results and interpretations

Reversals of reaction [M] were obtained at 500 MPa and 1 GPa, in T-$X^{Fl}_{H_2O}$ space. The 500 MPa results agree reasonably well with a reversal reported in Bohlen et al. (1983). However, due to a lack of experimental information on the mixing properties of H_2O–CO_2 fluids, we do not really know a_{H_2O}, and cannot yet extract reliable thermodynamic data from these experiments.

At the highest pressure investigated (1.5 GPa), we experienced a persistent experimental problem with the precipitation of graphite in the experimental charges. Since the exact f_{O_2} and f_{H_2} of the piston-cylinder assembly are unknown, we cannot attempt to calculate the actual fluid compositions in such experiments. Pilot runs have shown that it is possible to avoid graphite precipitation by packing a mixture of Fe_2O_3 and MgO around the sample capsule. The haematite acts as a hydrogen getter and induces highly oxidizing conditions in the assembly.

The results in Table 2 permit construction of isobaric T-$X^{Fl}_{H_2O}$ sections at 500 MPa and 1 GPa, with only reconnaissance results at 1.5 GPa (Figs. 10, 11). At 1 GPa, experiment K-92 (Table 2) was fortuitously conducted almost exactly at the inferred position of the isobaric invariant point. The run product contained the full six-phase invariant assemblage.

An important feature of Figs. 10 and 11 is that all melting equilibria shift to higher T in response to lowering of $X^{Fl}_{H_2O}$ (progressive addition of CO_2 to the system). The data constrain the locations of the equilibria sufficiently tightly that we can state unequivocally that there are no thermal minima in [En] and [Sa]. The inferred locations for the invariant points in these figures suggest that the univariant reaction (U) has a steep dP/dT slope and occurs at temperatures very similar to those of the fluid-absent reaction in $KAlO_2$–MgO–SiO_2–H_2O (see Fig. 12). Our data cannot directly constrain the stoichiometry of this reaction. However, its location at T higher than for [Sa] (and near [Fl] in K-AMSH) implies that the reaction is U_2, Phl + Qtz + Fl = En + Sa + M. By implication, alternative (b) (see

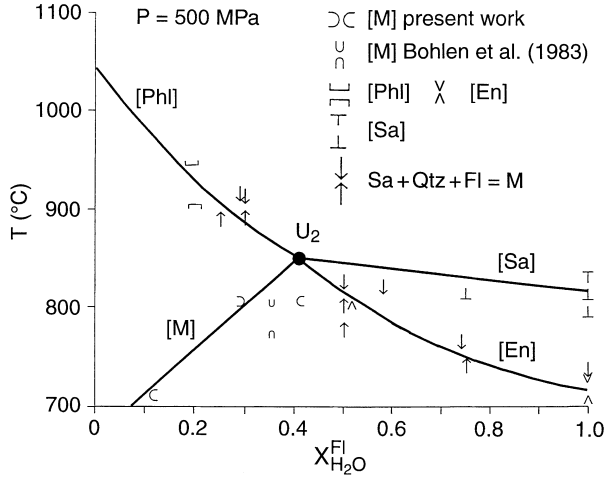

Fig. 10 T-$X^{Fl}_{H_2O}$ section at 500 MPa, constructed from the results of the present study (Table 2). Constraints on the locus of the reaction Sa + Qtz + Fl = M (Clemens 1981; Bohlen et al. 1983) are also shown, illustrating its proximity to [Phl] and [En]. The reversal of [M] reported by Bohlen et al. (1983) is also plotted

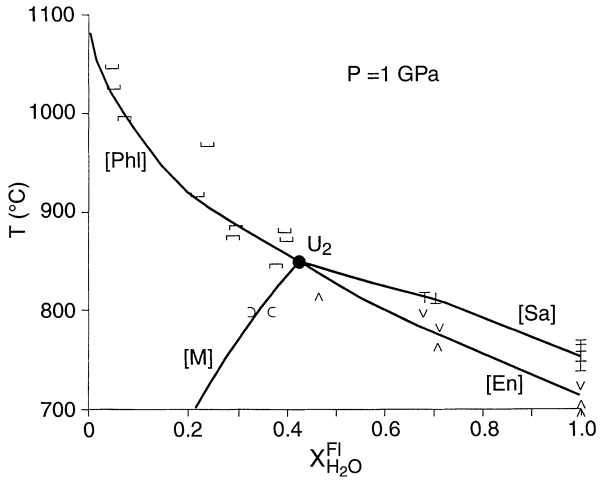

Fig. 11 T-$X^{Fl}_{H_2O}$ section at 1 GPa, constructed from the results of the present study (Table 2)

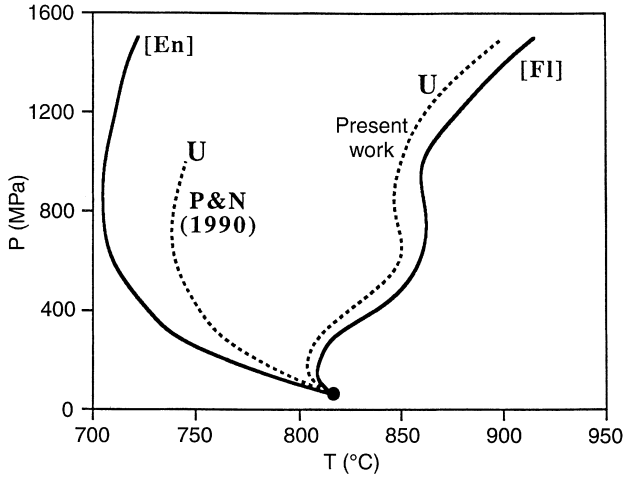

Fig. 12 P-T plot showing the loci of the reaction Phl + Qtz + Fl = En + Sa + M (U), according to Peterson and Newton (1990) and as inferred from the present work. The positions are approximate since the P&N curve is experimentally constrained only at 250 MPa and the present work only at 500 MPa and 1 GPa. However, this reaction must terminate at the invariant point (*black dot*) involving phlogopite, quartz, sanidine, enstatite and H_2O in the system $KAlO_2$–MgO–SiO_2–H_2O (Clemens 1995). For reference, the loci of the fluid-absent melting reaction Phl + Qtz = En + Sa + M ([Fl], Vielzeuf and Clemens 1992) and the enstatite-absent solidus Phl + Qtz + Sa + H_2O = M ([En], Clemens 1995) are also plotted. Since we infer that U lies close to [Fl], we show its slope changing in the same way as the well constrained slope changes in [Fl] (Vielzeuf and Clemens 1992)

Table 3 Electron probe analyses[a] (normalized wt% anhydrous) of some glasses (quenched melts) formed in the present experiments

Reaction	[Phl]	[Phl]	[Phl]	[Univariant]	[Sa]
Run no.	K-116	K-71	K-93	K-92	K-108
P (MPa)	502	998	1002	1003	1501
T (°C)	942	930	1025	850	840
$X^{Fl}_{H_2O}$	0.19	0.22	0.05	0.43	0.70
n	3	6	6	2	4
SiO_2	80.65 (0.47)	79.55 (0.88)	77.85 (0.69)	79.23 (0.80)	80.54 (0.56)
Al_2O_3	9.58 (0.33)	10.90 (0.51)	11.46 (0.42)	11.70 (0.35)	10.27 (0.02)
MgO	0.65 (0.11)	0.29 (0.20)	0.16 (0.04)	0.11 (0.11)	0.39 (0.06)
K_2O	9.11 (0.07)	9.24 (0.40)	10.53 (0.30)	8.96 (0.35)	8.81 (0.19)
Original total	93.90 (3.25)	94.77 (0.43)	93.71 (2.49)	94.71 (0.58)	92.25 (0.69)

[a] Specimens were cooled to liquid nitrogen temperature during analysis, to prevent counting losses on light elements. Numbers given are means of n individual analyses, with 1σ variations in parentheses

above and Figs. 4, 6) represents the true situation, with $X^{Fl}_{CO_2} >>> X^{M}_{CO_2} > 0$ (i.e. CO_2 only very slightly soluble in the melt phase at any given $X^{Fl}_{H_2O}$.

Table 3 shows data on the compositions of the glasses (quenched melts) obtained in some of the experiments. These melts were formed at temperatures between 840 and 1025 °C, with $X^{Fl}_{H_2O}$ varying from 0.05 to 0.70. Their compositions are "granitic", with high SiO_2 and never more than 0.65 wt% MgO. This is in accord with the proximity of [Phl] and [En] to Sa + Qtz + Fl = M in the MgO-free system K-ASH. There appears to be little consistent correlation between any compositional parameter and any intensive variable. The only such correlation may be that K_2O content appears to increase with T and decrease with $X^{Fl}_{H_2O}$.

There are important disparities between the results of Peterson and Newton (1989b, 1990) and the main body of other relevant experimental evidence. Comparison of the results of the present experiments with those of Peterson and Newton (both at $X^{Fl}_{H_2O} \approx 0.5$) shows that they report melting on [Sa] at a temperature about 100 °C lower than we find the solidus at 500 MPa and melting by [En] at least 160 °C below our inferred solidus at 1 GPa. Their inferred position for the univariant reaction at 600 MPa is about 110 °C below where we would place it (Figs. 10, 11). In addition, there are major discrepancies in melt compositions reported to coexist with quartz and the analytical data (Tables 2 – 4; Peterson and Newton 1990) show their melts to be silica undersaturated, containing normative olivine and leucite. Thus, they would seem to be well out of equilibrium with the solid phases with which they are reported to coexist. The highly magnesian (~20 wt% MgO) character of the melts is also at odds with their low-T origin. All petrological experience suggests that silicate melts only dissolve appreciable MgO at temperatures over 1000 °C. Peterson and Newton postulated that very Mg rich liquids could be metastable, because of kinetically inhibited growth of enstatite. However, pyroxenes nucleate and grow readily in high-P-T experiments, especially when a fluid is present and in mafic bulk compositions. Thus, inhibited enstatite growth is an unlikely explanation.

Geological implications

We find no evidence for any melt-fluxing effect of CO_2. On the contrary, as many previous experiments have shown, CO_2 inhibits fusion in hydrous silicate systems. Crustal melting in the presence of H_2O–CO_2 mixed fluids will always occur at higher temperatures than with pure H_2O fluid. Magmas produced by such melting will be granitic (s.l.), with relatively high SiO_2 and low MgO contents, irrespective of H_2O–CO_2 ratio in any coexisting fluid phase. They will not contain appreciable dissolved CO_2.

There is clear geological evidence that the passage of hot CO_2-rich fluids can cause local dehydration of the rocks through which they pass. Classic examples are the incipient "charnockites" (pyroxene-quartz-feldspar rocks) produced along fractures in biotite-bearing tonalitic to granitic gneisses in southern India (e.g. Janardhan et al. 1982; Stähle et al. 1987; Raith and Srikantappa 1993). Apart from H_2O loss, such reactions appear to be isochemical (e.g. Todd and Evans 1994). Supercritical crustal fluids, of all kinds, have low specific heat capacities compared to magmas. Thus, CO_2-rich fluid is unlikely to be a significant agent in heat advection or promotion of regional granulite-grade metamorphism, melting, magma generation, metasomatism or long-range silicate mass transfer in the crust.

What of the field evidence for an association between partial melting, charnockitization and the channellized flow of carbonic fluids? An "intimate relationship between the formation of charnockite and the production of anatectic granite" has been described at Kabbaldurga, India (Friend 1983). Koesterer et al. (1987) and Frost and Frost (1987) described veins of orthopyroxene-bearing granite (charnockite) cutting amphibolites in the Wind River Range of Wyoming. Surrounding the veins there are narrow zones within which the amphibolite-facies mineral assemblage is replaced by an orthopyroxene-bearing granulite-facies assemblage with a metamorphic fabric (non-igneous texture). These authors interpreted the granulite as an aureole surrounding the granite, and Frost and Frost (1987) described the

whole association as an example of partial melting due to CO_2-fluxed melting.

Based on the results presented here, we interpret such examples rather differently. Rock-fluid systems can be either fluid- or rock-dominated. In fluid-dominated systems, a copious supply of fluid will externally buffer the activities of volatile species in the system. In contrast, rock-dominated systems occur when the volume of any free fluid phase is too small to accomplish such external buffering and the fluid composition is controlled by redox, devolatilization or melting reactions. To explain the association between local melting, dehydration and the passage of CO_2-rich fluid, we need to consider what occurs in a rock-dominated system, with reference to Fig. 13.

During metamorphism, small quantities of CO_2 may be derived from local sources. Examples of such sources include exsolution from a crystallizing mafic magma, fluid transfer across lithological contacts with rocks undergoing decarbonation reactions, and oxidation of biogenic graphite in pelitic metasediments (by H_2O released in dehydration reactions or by reaction with Fe^{3+} in minerals). As demonstrated experimentally (Watson and Brenan 1987; Holness 1992), and in isotopic studies of precipitated graphite (e.g. Santosh and Wada 1993), CO_2-rich fluids do not wet grain boundaries in quartz-bearing crustal rocks; they migrate appreciable distances (> a few cm) by fracture pathways rather than by permeation (see also Todd and Evans 1994).

Channellized escape of such CO_2 could result in local dehydration in the wall rocks of the fractures (e.g. Fig. 13, point a). Breakdown of hydrous phases (e.g. biotite and hornblende) would dilute the carbonic fluid through release of H_2O, raising $X^{Fl}_{H_2O}$. If $X^{Fl}_{H_2O}$ rose sufficiently, under local disequilibrium conditions, the solidus of the host rock may be reached or overstepped (e.g. Fig. 13, point b). This would produce granitic partial melt that dissolved most of the H_2O in the fluid, eventually buffering fluid composition to that in equilibrium with granitic melt at the solidus (Fig. 13, point c). Escape of the fluid from the system, or retrograde cooling, would result in crystallization of the melt. The rock mass would then record a vein, filled with igneous-textured granitic material (which may still contain orthopyroxene, if T and $X^{Fl}_{H_2O}$ had been high enough to reach the [Sa] reaction), fringed by a narrow zone of granulite-facies rock with subsolidus, metamorphic textures. Such a feature could be misinterpreted as resulting from simple melt fluxing by CO_2-rich fluid. Although the proposed mechanism amounts to melting *triggered* by an influx of CO_2, this melting can only result through the occurrence of local disequilibrium and does not involve melting *fluxed* by CO_2.

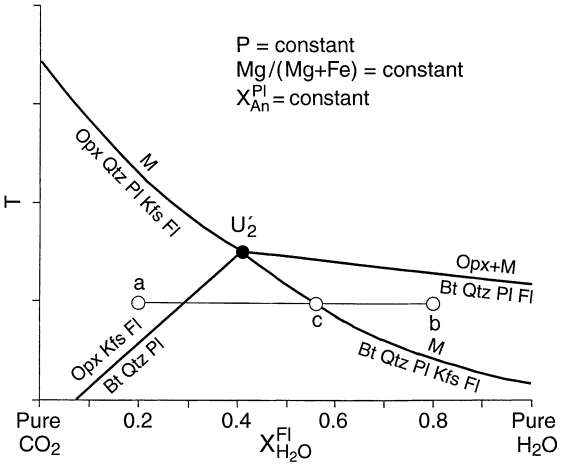

Fig. 13 Hypothetical T-$X^{Fl}_{H_2O}$ section through the system $KAlO_2$–$NaAlO_2$–MgO–FeO–SiO_2–H_2O–CO_2 (modelled on relations in K-AMSHC at 500 MPa) illustrating the possible isothermal evolution of a K-feldspar-free, biotite-quartz-bearing rock (e.g. metatonalite), with a small quantity of an initially CO_2-rich fluid present. Note that the equilibria shown as lines here would actually be narrow polyvariant bands (e.g. Carrington and Harley 1995); U′$_2$ (analogue of U_2 in Fig. 10) would actually be a small divariant field. These complications are omitted for clarity. At point *a* the carbonic fluid is introduced at a temperature too low to permit melting. However, biotite breaks down in the subsolidus to yield K-feldspar and progressively enrich the fluid in H_2O. Provided that the dehydration rate is sufficiently fast, the disequilibrium fluid composition may locally evolve toward a point such as *b*, where partial melting would take place. With the passage of sufficient time, resumption of equilibrium conditions would occur, with a shift in fluid composition to that at point *c*, on the fluid-saturated solidus. Here the system would remain until cooling or fluid escape caused the melt to crystallize.

Acknowledgements Some of the 500 MPa experiments described here, were performed at Monash university, in Australia, forming part of the Ph.D. research of J.D.C. These were funded through Australian Research Grants Committee grant E74/15102 to Dr V. J. Wall. Unit-cell parameters for synthetic phlogopite and enstatite were determined by Mr. Y. Blanc at CNRS URA10, Clermont-Ferrand, France. New experiments at 1 and 1.5 GPa (as well as a few at lower pressure) were performed at Manchester University with funding from NERC research grant GR3/7669, to J.D.C. The rest of the low-pressure work was carried out in the experimental petrology laboratory at Clermont-Ferrand, while J.D.C. was employed there as Directeur de Recherche Associé. Figures 1 to 6 were drafted by Mr. R. Hartley at Manchester University. The paper benefited from incisive and critical reviews by Prof. Simon Harley and Dr. Alberto Patiño Douce.

Appendix

$X^{Fl}_{H_2O}$ in 500 MPa experiments with precipitated graphite

For two of the 500 MPa experiments (K-135 and K-136) with "H_2O–CO_2" fluid phases (Clemens 1981), the run products included some graphite. The C–H–O system is invariant at fixed P, T and f_{H_2O} with $a_{graphite} = 1$. Thus, assuming equilibrium was attained, the fluid compositions in these experiments were buffered. To calculate $X^{Fl}_{H_2O}$ we used expressions for the equilibrium constants of various reactions in the graphite-fluid system (Ohmoto and Kerrick 1977). We made two additional assumptions: (1) that $P_{total} = P_{H_2O} + P_{H_2} + P_{CO_2} + P_{CO} + P_{CH_4}$, i.e. we neglected the very small partial pressure of O_2; (2) that the fluid species mixed ideally ($a = X$).

Initial data include: P_{total} = 504 MPa, T = 717 °C, f_{H_2} = 4.6 MPa (imposed with the H_2 membrane) and a_c = 1

(graphite stable). We used Γ_{H_2O} from Burnham et al. (1969), Γ_{CO_2} from Shmulovich and Shmonov (1978) and Γ_{H_2} and γ_{CH_4} from Ryzhenko and Volkov (1971). Results indicate that $X^{Fl}_{H_2O} = 0.104$, $X^{Fl}_{H_2} = 0.003$, $X^{Fl}_{CO_2} = 0.879$, $X^{Fl}_{CO} = 0.004$ and $X^{Fl}_{CH_4} = 0.010$. Note that the modified Redlich-Kwong equation of state for H_2O–CO_2 mixtures (Kerrick and Jacobs 1981) predicts small positive deviations from ideal mixing. Such non-ideality would have essentially negligible effects on the calculated mole fractions of the fluid species. Ulmer and Luth (1991) published an experimentally based equation for calculating f_{O_2} as a function of P and T in the graphite-COH system. This can be used as a rough check on the above calculation. Assuming ideality in the fluid phase, at the above experimental conditions, the calculated $X^{Fl}_{H_2O}$ is 0.12 ± 0.03. This is surprisingly close to the value obtained above, given the assumptions and that the Ulmer and Luth equation is strictly valid only for P between 1 and 3 GPa.

References

Beard JS, Lofgren GE (1991) Dehydration melting and water-saturated melting of basaltic and andesitic greenstones and amphibolites at 1, 3, and 6.9 kbar. J Petrol 32: 365–401

Blank JG, Stolper EM, Carroll MR (1993) Solubilities of carbon dioxide and water in rhyolitic melt at 850 °C and 750 bars. Earth Planet Sci Lett 119: 27–36

Bohlen SR, Boettcher AL (1982) The quartz ↔ coesite transformation: a precise determination and the effects of other components. J Geophys Res 87: 7073–7078

Bohlen SR, Boettcher AL, Wall VJ, Clemens JD (1983) Stability of phlogopite–quartz and sanidine–quartz: a model for melting in the lower crust. Contrib Mineral Petrol 83: 270–277

Burnham CW (1962) Large volume apparatus for hydrothermal investigations to 10,000 bars and 1500 °C (abstract). Am Ceram Soc Program, Seattle, Washington, unpaginated

Burnham CW, Holloway JR, Davis NF (1969) Thermodynamic properties of water to 1000 °C and 10,000 bars. Geol Soc Am Spec Pap 132: 96

Carrington DP, Harley SL (1995) Partial melting and phase relations in high-grade metapelites – a experimental petrogenetic grid in the KFMASH system. Contrib Mineral Petrol 120: 270–291

Carrington D, Harley S (1996) Cordierite as a monitor of fluid and melt H_2O contents in the lower crust. Geology 24: 647–650

Carroll MR, Holloway JR (1994) Volatiles in magmas. (Reviews in mineralogy, vol 30) Mineral Soc Am, Washington, DC

Circone S, Navrotsky A (1992) Substitution of $^{[6,4]}$Al in phlogopite: high-temperature solution calorimetry, heat capacities, and thermodynamic properties of the phlogopite-eastonite join. Am Mineral 77: 1191–1205

Clemens JD (1981) Origin and evolution of some peraluminous acid magmas. PhD thesis, Monash Univ, Clayton, Victoria, Australia

Clemens JD (1990) The granulite – granite connexion. In: Vielzeuf D, Vidal P (eds) Granulites and crustal differentiation. Kluwer Academic Publishers, Dordrecht, pp 25–36

Clemens JD (1993) Experimental evidence against CO_2-promoted deep crustal melting. Nature 363: 336–338

Clemens JD (1995) Phlogopite stability in the silica-saturated portion of the system $KAlO_2 - MgO - SiO_2 - H_2O$: new data and a reappraisal of phase relations to 1.5 GPa. Am Mineral 80: 982–997

Clemens JD, Circone S, Navrotsky A, McMillan PF, Smith B, Wall VJ (1987) Phlogopite: new calorimetric data and the effect of stacking disorder on thermodynamic properties. Geochim Cosmochim Acta 51: 2569–2578

Collerson KD, Fryer BJ (1978) The role of fluids in the formation and subsequent development of the early crust. Contrib Mineral Petrol 67: 151–167

Edwards RL, Essene EJ (1988) Pressure, temperature and C–O–H fugacities across the amphibolite-granulite transition NW Adirondack mountains, NY. J Petrol 29: 39–72

Eggler DH, Kadik AA (1979) The system $NaAlS_2O_8 - H_2O - CO_2$ to 20 kbar pressure. I. Compositional and thermodynamic relations of liquids and vapors coexisting with albite. Am Mineral 64: 1036–1048

Esperança S, Holloway JR (1986) The origin of the high-K latites from Camp Creek, Arizona: constraints from experiments with variable f_{O_2} and a_{H_2O}. Contrib Mineral Petrol 93: 504–512

Fogel RA, Rutherford MJ (1990) The solubility of carbon dioxide in rhyolitic melts: a quantitative FTIR study. Am Mineral 75: 1311–1326

Friend CRL (1983) The link between charnockite formation and granite production: evidence from Kabbaldurga, Karnatarka, southern India. In: Atherton MP, Gribble CD (eds) Migmatites, melting and metamorphism. Shiva Publishing Ltd. Nantwich, pp 264–276

Frost BR, Frost CD (1987) CO_2, melts and granulite metamorphism. Nature 327: 503–506

Fyfe WS (1973) The granulite facies, partial melting and the Archean crust. Philol Trans R Soc London A273: 457–461

Grant JA (1985) Phase-equilibria in low-pressure partial melting of pelitic rocks. Am J Sci 285: 409–435

Grant JA (1986) Quartz-phlogopite-liquid equilibria and origins of charnockites. Am Mineral 71: 1071–1075

Hall DL, Sterner SM (1993) Preferential water loss from synthetic fluid inclusions. Contrib Mineral Petrol 114: 489–500

Hewitt DA, Wones DR (1984) Experimental phase-relations of the micas. In: Bailey SW (ed) Micas. (Reviews in mineralogy, vol 13) Mineral Soc Am, Washington, DC, pp 201–256

Hollister LS (1988) On the origin of CO_2-rich fluid inclusions in migmatites. J Metamorphic Geol 6: 467–474

Holloway JR, Jakobsson S (1986) Volatile solubilities in magmas: transport of volatiles from mantles to planet surfaces. J Geophys Res B91: D505–D508

Holloway JR, Pan V, Gudmundsson G (1992) High-pressure fluid-absent melting experiments in the presence of graphite: oxygen fugacity, ferric/ferrous ratio and dissolved CO_2. Eur J Mineral 4: 105–114

Holness MB (1992) Equilibrium dihedral angles in the system quartz–CO_2–H_2O–NaCl at 800 °C and 1–15 kbar – the effects of pressure and fluid composition on the permeability of quartzites. Earth Planet Sci Lett 114: 171–184

Holness MB, Graham CM (1991) Equilibrium dihedral angles in the system H_2O–CO_2–NaCl–calcite and implications for fluid flow during metamorphism. Contrib Mineral Petrol 108: 368–383

Jakobsson S, Holloway JR (1986) Crystal-liquid experiments in the presence of a C–O–H fluid buffered by graphite + iron + wustite: experimental method and near-liquidus relations in basanite. J Volcanol Geothermal Res 29: 265–291

Janardhan AS, Newton RC, Hansen EC (1982) The transformation of amphibolite facies gneiss to charnockite in southern Karnataka and northern Tamil Nadu, India. Contrib Mineral Petrol 79: 130–149

Kerrick DM, Jacobs GK (1981) A modified Redlich-Kwong equation of state for H_2O, CO_2 and H_2O–CO_2 mixtures at elevated pressures and temperatures. Am J Sci 281: 735–767

Koesterer ME, Frost CD, Frost BR, Hulesbosch TP (1987) Development of the Archean crust in the Medina Mountain area, Wind River Range, Wyoming (U.S.A.). Precambrian Res 37: 287–304

Kretz R (1983) Symbols for rock-forming minerals. Am Mineral 68: 277–279

Lamb W, Valley JW (1984) Metamorphism of reduced granulites in low-CO_2 vapor-free environment. Nature 312: 56–58

LeBreton N, Thompson AB (1988) Fluid-absent (dehydration) melting of biotite in metapelites in the early stages of crustal anatexis. Contrib Mineral Petrol 99: 226–237

Luth WC (1967) Studies in the system $KAlSiO_4 - Mg_2SiO_4 - SiO_2 - H_2O$. I. inferred phase relations and petrologic application. J Petrol 8: 372–416

Montana A, Brearley M (1989) An appraisal of the stability of phlogopite in the crust and the mantle. Am Mineral 74: 1–4
Mysen BO, Arculus RJ, Eggler DH (1975) Solubility of carbon dioxide in melts of andesite, tholeiite and olivine nephelinite composition to 30 kbar pressure. Contrib Mineral Petrol 53: 227–239
Newton RC (1990) Fluids and melting in the Archaean deep crust of southern India. In: Ashworth JR, Brown M (eds) High-temperature metamorphism and crustal anatexis. Unwin-Hyman, London, pp 149–179
Newton RC, Smith JV, Windley BF (1980) Carbonic metamorphism, granulites and crustal growth. Nature 288: 45–50
Ohmoto H, Kerrick D (1977) Devolatilization equilibria in graphitic systems. Am J Sci 277: 1013–1044
O'Neill HSC (1987) Quartz-fayalite-iron and quartz-fayalite-magnetite equilibria and the free energy of formation of fayalite (Fe_2SiO_4) and magnetite (Fe_3O_4). Am Mineral 72: 67–75
Patiño Douce AE, Beard JS (1995) Dehydration-melting of biotite gneiss and quartz amphibolite from 3 to 15 kbar. J Petrol 36: 707–738
Patiño Douce AE, Beard JS (1996) Effects of P, f_{O_2} and Mg/Fe ratio on dehydration melting of model metagraywackes. J Petrol 37: 999–1024
Patiño Douce AE, Johnston AD (1991) Phase equilibria and melt productivity in the pelitic system: implications for the origin of peraluminous granitoids and aluminous granulites. Contrib Mineral Petrol 107: 202–218
Pawley AR, Holloway JR, McMillan PF (1992) The effect of oxygen fugacity on the solubility of carbon-oxygen fluids in basaltic melt. Earth Planet Sci Lett 110: 213–225
Peterson JW, Newton RC (1989a) CO_2-enhanced melting of biotite-bearing rocks at deep-crustal pressure-temperature conditions. Nature 340: 378–380
Peterson JW, Newton RC (1989b) Reversed experiments on biotite-quartz-feldspar melting in the system KMASH: implications for crustal anatexis. J Geol 97: 465–485
Peterson JW, Newton RC (1990) Experimental biotite-quartz melting in the KMASH-CO_2 system and the role of CO_2 in the petrogenesis of granites and related rocks. Am Mineral 75: 1029–1042
Phillips GN (1980) Water activity changes across an amphibolite-granulite facies transition, Broken Hill, Australia. Contrib Mineral Petrol 75: 377–386
Powell R, Downes J (1990) Garnet porphyroblast-bearing leucosomes in metapelites: mechanisms, phase diagrams, and an example from Broken Hill, Australia. In: Ashworth JR, Brown M (eds) High-temperature metamorphism and crustal anatexis. Unwin-Hyman, London, pp 105–123
Raith M, Srikantappa C (1993) Arrested charnockite formation at Kottavattam, southern India. J Metamorphic Geol 11: 815–832
Rapp RP, Watson EB (1995) Dehydration melting of metabasalt at 8–32 kbar: implications for continental growth and crust-mantle recycling. J Petrol 36: 891–931
Rapp RP, Watson EB, Miller CF (1991) Partial melting of amphibolite/eclogite and the origin of Archean trondhjemites and tholeiites. Precambrian Res 51: 1–25
Robie RA, Hemingway BS (1984) Heat capacities and entropies of phlogopite ($KMg_3[AlSi_3O_{10}](OH)_2$) and paragonite ($NaAl_2[AlSi_3O_{10}](OH)_2$) between 5 and 900 K and estimates of the enthalpies and Gibbs free energies of formation. Am Mineral 69: 858–868
Rudnick RL, Ashwal LD, Henry DI (1984) Fluid inclusions in high-grade gneisses of the Kapuskasing structural zone, Ontario: metamorphic fluids and uplift erosion path. Contrib Mineral Petrol 87: 399–406
Rushmer T (1991) Partial melting of 2 amphibolites – contrasting experimental results under fluid-absent conditions. Contrib Mineral Petrol 107: 41–59
Rutter MJ, Wyllie PJ (1988) Melting of vapour-absent tonalite at 10 kbar to simulate dehydration-melting in the deep crust. Nature 331: 159–160
Ryzhenko BN, Volkov VP (1971) Fugacity coefficients of some gasses in a broad range of temperatures and pressures. Geochem Int 1971: 468–481
Santosh M, Wada H (1993) Microscale isotopic zonation in graphite crystals: evidence for channelled CO_2 influx in granulites. Earth Planet Sci Lett 119: 19–26
Sen C, Dunn T (1994) Dehydration melting of a basaltic composition amphibolite at 1.5 and 2.0 GPa: implications for the origin of adakites. Contrib Mineral Petrol 117: 394–409
Shmulovich KI, Shmonov VM (1978) Carbon dioxide (in Russian). (Tables of thermodynamic properties of gasses and liquids, vol 3. Isdatelstvo Standartov, Moscow
Sighinolfi GP, Gorgoni C (1978) Chemical evolution of high-grade metamorphic rocks – anatexis and remotion of material from granulite terranes. Chem Geol 22: 157–176
Skjerlie S, Johnston AD (1993) Fluid-absent melting behaviour of an F-rich tonalitic gneiss at mid-crustal pressures: implications for the generation of anorogenic granites. J Petrol 34: 785–815
Stähle HJ, Raith M, Hoernes S, Delfs A (1987) Element mobility during incipient granulite formation at Kabbaldurga, southern India. J Petrol 28: 803–834
Stevens G, Clemens JD (1993) Fluid-absent melting and the roles of fluids in the lithosphere: a slanted summary? Chem Geol 108: 1–17
Stevens G, Clemens JD, Droop GTR (1995) Hydrous cordierite in granulites: experiments and implications for crustal magmatism. Geology 23: 925–928
Stevens G, Van Reenen DD (1992) Partial melting and the origin of the metapelitic granulites in the Southern Marginal Zone of the Limpopo Belt, South Africa. Precambrian Res 55: 303–319
Todd CS, Evans BW (1994) Properties of CO_2-induced dehydration of amphibolite. J Petrol 35: 1213–1239
Touret JLR (1970) Le faciès granulite, métamorphisme en milieu carbonique. CR Acad Sci Paris D 271: 2228–2231
Touret JLR (1971) Le faciès granulite en Norvège Meridonale. II. Les inclusions fluides. Lithos 4: 423–436
Touret JLR (1985) Fluid regime in southern Norway: the record of fluid inclusions. In: Tibi AC, Touret JLR (eds) The deep Proterozoic crust in the N. Atlantic Provinces. D Reidel, Dordrecht, pp 517–549
Ulmer P, Luth RW (1991) The graphite-COH fluid equilibrium in P, T, f_{O_2} space: an experimental determination to 30 kbar and 1600 °C. Contrib Mineral Petrol 106: 265–272
Valley JW, Bohlen SR, Essene EJ, Lamb W (1990) Metamorphism in the Adirondacks. II. The role of fluids. J Petrol 31: 555–596
Venneman TW, Smith HS (1992) Stable isotope profile across the orthopyroxene isograd in the Southern Marginal Zone of the Limpopo Belt, South Africa. Precambrian Res 55: 365–398
Vielzeuf D, Clemens JD (1992) Fluid-absent melting of phlogopite + quartz: experiments and models. Am Mineral 77: 1206–1222
Vielzeuf D, Holloway JR (1988) Experimental determination of the fluid-absent melting reactions in the pelitic system: consequences for crustal differentiation. Contrib Mineral Petrol 98: 257–276
Vielzeuf D, Montel J-M (1994) Partial melting of metagreywackes. 1. Fluid-absent experiments and phase relationships. Contrib Mineral Petrol 117: 375–393
Watson EB, Brenan JM (1987) Fluids in the lithosphere. 1. Experimentally determined wetting characteristics of CO_2–H_2O fluids and their implications for fluid transport, host-rock physical properties and fluid inclusion formation. Earth Planet Sci Lett 85: 497–515
Wendlandt RF (1981) Influence of CO_2 on melting of model granulite facies assemblages: a model for the genesis of charnockites. Am Mineral 66: 1164–1174
Wendlandt RF, Eggler DH (1980a) The origins of potassic magmas. 1. Melting relations in the systems $KAlSiO_4-Mg_2SiO_4-SiO_2$ and $KAlSiO_4-MgO-SiO_2-CO_2$ to 30 kilobars. Am J Sci 280: 345–420

Wendlandt RF, Eggler DH (1980b) The origins of potassic magmas. 2. Stability of phlogopite in natural spinel lherzolite and in the system $KAlSiO_4 - MgO - SiO_2 - H_2O - CO_2$ at high pressures and temperatures. Am J Sci 280: 421–458

Wones DR, Dodge FCW (1977) The stability of phlogopite in the presence of quartz and diopside. In: Fraser DG (ed) Thermodynamics in geology, D. Reidel, Dordrecht, pp 229–247

Wright TL (1968) X-ray and optical study of alkali feldspar. II. An X-ray method for determining the composition and structural state from measurement of 2θ values from three reflections. Am Mineral 53: 88–104

Zen E-an (1966) Construction of pressure-temperature diagrams for multicomponent systems after the method of Schreinemakers – a geometric approach. U S Geol Surv Bull 1225